AGU100 ADVANCING EARTH AND SPACE SCIENCE

Water Resources Research

RESEARCH ARTICLE
10.1029/2017WR022108

A Modeling Study of Direct and Indirect N_2O Emissions From a Representative Catchment in the U.S. Corn Belt

Congsheng Fu[1,2,3], Xuhui Lee[1,3], Timothy J. Griffis[4], John M. Baker[4,5], and Peter A. Turner[4]

[1]Yale-NUIST Center on Atmospheric Environment, Nanjing University of Information Science & Technology, Nanjing, China, [2]Key Laboratory of Watershed Geographic Sciences, Nanjing Institute of Geography and Limnology, Chinese Academy of Sciences, Nanjing, China, [3]School of Forestry and Environmental Studies, Yale University, New Haven, CT, USA, [4]Department of Soil, Water, and Climate, University of Minnesota, Saint Paul, MN, USA, [5]United States Department of Agriculture, Agricultural Research Service, Saint Paul, MN, USA

Key Points:
- Zero-order streams are N_2O emission hot spots in the Corn Belt
- The IPCC N_2O emission factor for streams in the Corn Belt should be increased by 3.2–5.7 times
- Increasing precipitation and streamflow in the Corn Belt may potentially increase N_2O emissions from both soils and streams

Supporting Information:
- Supporting Information S1

Correspondence to:
X. Lee,
xuhui.lee@yale.edu;
C. Fu,
congsheng.fu@yale.edu

Citation:
Fu, C., Lee, X., Griffis, T. J., Baker, J. M., & Turner, P. A. (2018). A modeling study of direct and indirect N_2O emissions from a representative catchment in the U.S. Corn Belt. *Water Resources Research*, *54*, 3632–3653. https://doi.org/10.1029/2017WR022108

Received 24 OCT 2017
Accepted 12 APR 2018
Accepted article online 17 APR 2018
Published online 21 MAY 2018

Abstract Indirect nitrous oxide (N_2O) emissions from drainage ditches and headwater streams are poorly constrained. Few studies have monitored stream N_2O emissions and fewer modeling studies have been conducted to simulate stream N_2O emissions. In this study, we developed direct and indirect N_2O emission modules and a corresponding calibration module for use in the Soil and Water Assessment Tool (SWAT) model, and implemented the expanded SWAT model (termed SWAT-N_2O) to a representative fourth-stream-order catchment (210 km^2) and six first-order stream catchments (0.22–1.83 km^2) in southeastern Minnesota. We simulated the spatial and temporal fluctuations of the indirect emissions from streams, identified emission "hot spots" and "hot moments," and diagnosed the correlations between direct and indirect emissions. We showed that zero-order streams and first-order streams could contribute 0.034–0.066 and 0.011 nmol N_2O m^{-2} s^{-1} (expressed on the basis of unit catchment area) to the total surface emissions, respectively. Emissions from zero-order and first-order streams equal 24–41% of direct emissions from soil, which may explain the emission gap between calculations using top-down and bottom-up methods. Clear spatial patterns were identified for both direct and indirect emissions and their spatial variations were negatively correlated. Our results suggest that the IPCC N_2O emission factor for streams in the Corn Belt should be increased by 3.2–5.7 times. Increasing precipitation and streamflow in the Corn Belt may potentially increase frequencies of soil anoxic conditions and nitrate leaching to streams, and subsequently increase N_2O emissions from both soils and streams.

1. Introduction

Nitrous oxide (N_2O) is the dominant stratospheric ozone depleting substance (Ravishankara et al., 2009), and has a radiative forcing that ranks third among the long-lived greenhouse gases (Hofmann et al., 2006). Nitrous oxide is inert in the troposphere with a lifetime exceeding one hundred years (Prather et al., 2012, 2015). The globally averaged atmospheric N_2O concentration has been steadily increasing at a rate of 0.7–0.8 ppb yr^{-1} since the late-1970s (Denman et al., 2007; Hall et al., 2007; Saikawa et al., 2014).

The U.S. Corn Belt (scope shown in Figure 1a), an intensively managed agricultural region with 6.2 Tg of N fertilizer applied to fields each year (Griffis et al., 2017), plays an important role in the global anthropogenic N_2O budget. Currently, the emission determined with top-down methods is larger than that with bottom-up methods for the Corn Belt (Chen et al., 2016; Griffis et al., 2013; Miller et al., 2012). Top-down methods use atmospheric concentration data and a transport model to determine the surface N_2O emissions. Bottom-up methods calculate the emissions as the multiplication of nitrogen fertilizer input or relevant activity strength with predetermined emission factors (De Klein et al., 2006).

Nitrous oxide emissions to the atmosphere from soils are defined as "direct emissions," and emissions at downstream distances from the point of fertilizer application and other activity (e.g., emissions from ditches and streams due to leaching and runoff of N fertilizer, manure and residue) are defined as "indirect emissions" (De Klein et al., 2006). Indirect emissions, which are principally caused by two microbial transformations—denitrification and nitrification, account for over 1/4 of the global total agricultural N_2O emissions

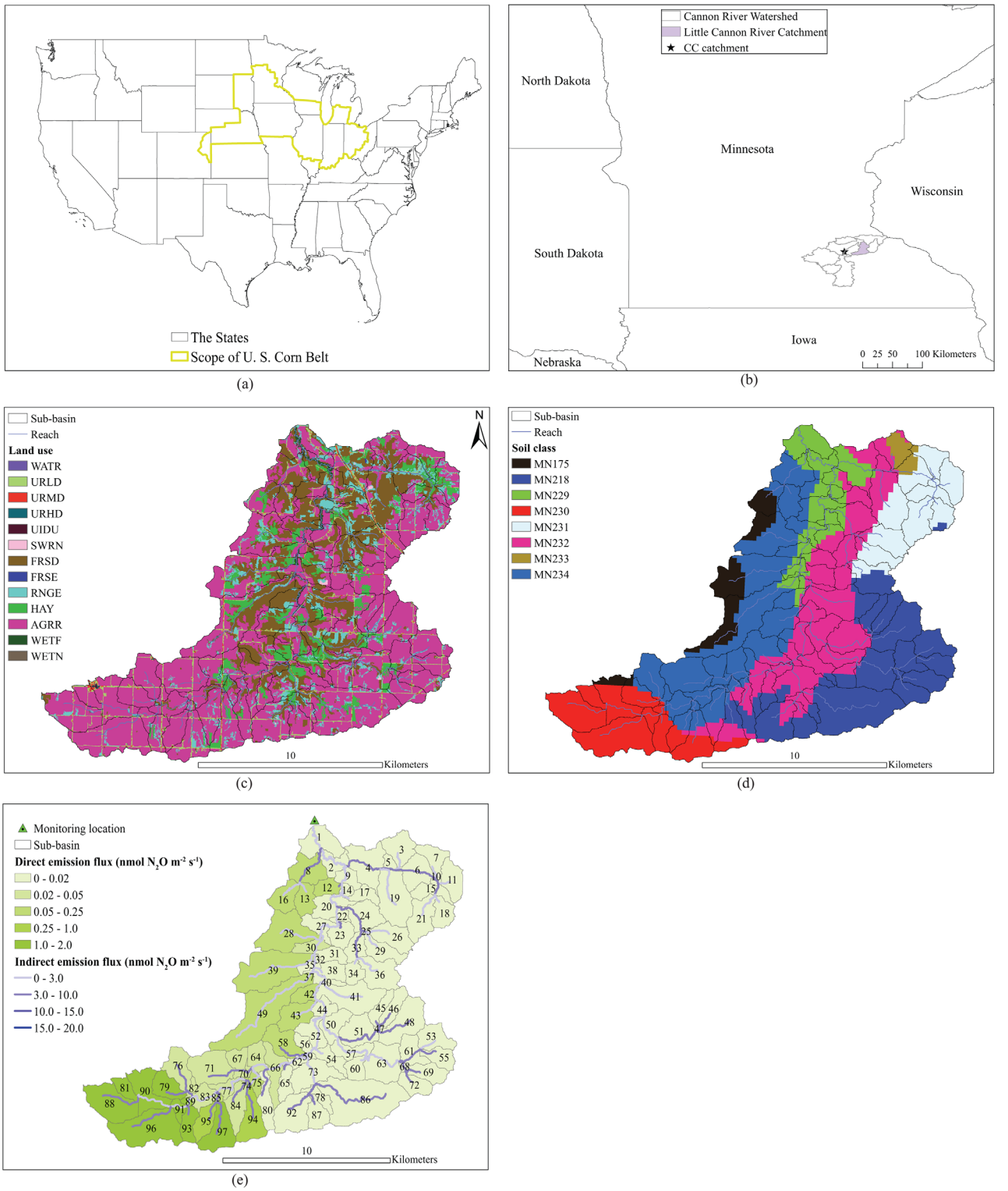

Figure 1. Locations of the (a) U. S. Corn Belt and (b) the studied catchments, (c) land use, (d) soil classes, and (e) modeled direct and indirect N_2O emission fluxes of the studied Little Cannon River catchment. Numbers in plot (e) are subbasin's IDs. CC in plot (b) is one of first-order stream catchments where stream N_2O emission fluxes were monitored. WATR: Water; URLD: Residential-Low Density; URMD: Residential-Medium Density; URHD: Residential-High Density; UIDU: Industrial; SWRN: South Western Range; FRSD: Deciduous Forest; FRSE: Evergreen Forest; RNGE: Grasslands/Herbaceous; HAY: Hay; AGRR: Agricultural Land-Row Crops; WETF: Woody Wetlands; WETN: Emergent/Herbaceous Wetlands; MN175: Ostrander; MN218: Seaton; MN229: Estherville; MN230: Maxfield; MN231: Frontenac; MN232: Marlean; MN233: Timula; MN234: Garwin.

(Reay et al., 2012; Snider et al., 2015). Rivers remain a major uncertain N_2O source in the world (Beaulieu et al., 2010, 2011), due to high variability of surface water N_2O concentrations, limited number of samples, and low spatiotemporal sampling resolutions in monitoring stream water chemistry and turbulence (Nevison, 2000). Recent studies have shown that indirect emissions from drainage ditches and streams in the Corn Belt are underestimated. Turner et al. (2015) measured N_2O emissions from streams of first to ninth Strahler orders in Minnesota, and reported that the Intergovernmental Panel on Climate Change (IPCC) indirect emissions from streams and rivers were underestimated by up to nine fold. Using the Stochastic Time-Inverted Lagrangian Transport (STILT) model and a Bayesian inversion technique, Chen et al. (2016) reported that the indirect emissions from the Corn Belt were 1.9–4.6 times as large as those suggested for indirect emissions from streams and rivers by the IPCC inventory methodology.

The number of field studies that directly measure stream/river N_2O emissions with chambers is growing quickly (Beaulieu et al., 2010; Chen et al., 2015; Clough et al., 2006a; Grossel et al., 2016; Harrison & Matson, 2003; Hinshaw & Dahlgren, 2013; McMahon & Dennehy, 1999; Turner et al., 2015), and more studies have calculated stream N_2O emissions using simple air-water gas exchange models (Baulch et al., 2011, 2012; Beaulieu et al., 2011; Clough et al., 2006a, 2006b, 2007; Gardner et al., 2016; Garnier et al., 2009; Harrison et al., 2005; Harrison & Matson, 2003; Hinshaw & Dahlgren, 2013; Laursen & Seitzinger, 2004; Marzadri et al., 2014, 2017; Reay et al., 2003; Rosamond et al., 2012; Soued et al., 2016; Yan et al., 2012) or process-based models (Marzadri et al., 2011). We are not aware of watershed-scale modeling studies on stream N_2O emissions that combine land and stream processes in the published literature. Watershed-scale models may be a powerful tool for diagnosing the mechanisms of N_2O emissions, including the total flux, its temporal fluctuations and spatial characteristics, and the correlation between direct and indirect emissions. The lack of watershed-scale modeling studies on indirect N_2O emissions from streams may have been caused by the different focus between hydrologists and atmospheric scientists. Hydrologists have conducted numerous modeling studies on stream nitrate concentration ($[NO_3^-]$), mainly for the purpose of protection of water quality (e.g., Wellen et al., 2015), but few have paid attention to $[NO_3^-]$-related stream N_2O emissions. On the other hand, atmospheric researchers have developed models for stream N_2O emissions (e.g., Chen et al., 2016; Oleson et al., 2013), but their models do not explicitly calculate stream $[NO_3^-]$ and are usually based on latitude and longitude grids instead of detailed watershed units more suitable for analyzing N cycling (Beaulieu et al., 2011; Garnier et al., 2009).

A robust watershed-scale N_2O model should account for drivers of N cycling processes in soils and in waterways. Field experiments demonstrate the importance of soil texture in direct N_2O emissions. Generally, the direct N_2O emissions increase with clay content in the soil in most cases because anaerobic denitrification occurs more frequently in fine-textured soils than in coarse-textured soils (Gaillard et al., 2016; Skiba & Ball, 2002). Drainage conditions also affect direct N_2O emissions through their influence on soil oxygen levels and N loss via leaching (Grossel et al., 2016).

Field observations illustrate that although other environmental variables such as dissolved oxygen in water (Rosamond et al., 2012), water temperature (Venkiteswaran et al., 2014), and residence time (Marzadri et al., 2014; Quick et al., 2016) influence stream N_2O emissions, $[NO_3^-]$ is the dominant control on stream N_2O concentration ($[N_2O]$) and emissions (Baulch et al., 2011; Beaulieu et al., 2010, 2011; Chen et al., 2015; Turner et al., 2016). Furthermore, Turner et al. (2015) reported that first Strahler order streams, and potentially zero-order streams are emission hot spots in the Corn Belt. Zero-order streams, are highly episodic drainage ditches or microflow stream channels extending upland of headwater streams, and they are the smallest stream channels in the stream network. The N_2O transfer velocity, or the rate of N_2O exchange between stream water and the atmosphere, is controlled by turbulent flow that is influenced by stream geometry (width, depth, and slope; Raymond et al., 2012).

This study develops a watershed-scale model that fully integrates nitrogen cycles in land soils and streams, and the latter is affected by stream hydraulic geometry and collecting area (or Strahler order). Our model, SWAT-N_2O, is an extension of the semidistributed Soil and Water Assessment Tool (SWAT; Arnold et al., 1998). SWAT is a widely used soil and water management model, and more than 2,700 academic papers have been published on SWAT applications (Center for Agricultural and Rural Development (CARD), 2017). In the present study, we use SWAT-N_2O to simulate the direct and indirect N_2O emissions from one fourth-order and six first-order stream catchments in southeastern Minnesota, USA. These catchments have a land use pattern typical of the U.S. Corn Belt. Our goals are to quantify spatial and temporal fluctuations of the

indirect emissions from streams, including zero-order and first-order streams, to identify "hot spots" and "hot moments" of emissions in the catchment, and to analyze the relationships between direct and indirect emissions at the subcatchment scale.

2. Material and Methods

2.1. Study Sites and Data

This study focuses on the Little Cannon River Catchment (hereafter LCRC; area 210 km^2), which is located ~50 km south of Minneapolis-Saint Paul, Minnesota and is a part of the Cannon River watershed (Figure 1b). Agricultural crops, deciduous forest, and grassland make up 57.1%, 25.2%, and 15.8% of the catchment, respectively. Other components, such as urban (1.0%) and wetlands (<1%), occupy minor fractions (Figure 1c). Most of the catchment is within the ecoregion that underwent limited landscape formation by glacial ice, and the resulting landscape is mostly gently sloping to rolling summits that create scenic landscapes of deep valleys, abundant rock outcrops, high bluffs, caves, crevices, and sinkholes. Limestone and sandstone outcrops are observed along some streams and rivers (National Resource Conservation Service (NRCS), 2006). Soil textures in the LCRC are mainly loam, silt loam, and silty clay loam, while soil depth varies from

Table 1
Parameters of SWAT and Corresponding Ranges for Calibration and Validation

Module	Parameters	Meaning	Min_value	Max_value	Exp1	Exp2
Interception	*Canmx*	Maximum canopy storage (mm)	0	5.0	2.43	2.43
Snowmelt	*Sftmp*	Snowfall temperature (°C)	0	3.0	0.094	0.094
	Smtmp	Snow melt base temperature (°C)	0	3.0	0.82	0.82
	Smfmx	Maximum snowmelt factor for June 21 (mm H_2O/°C day)	0	12.0	9.63	9.63
	Smfmn	Maximum snowmelt factor for December 21 (mm H_2O/°C day)	0	12.0	4.05	4.05
	Timp	Snow pack temperature lag factor	0	1.0	0.092	0.092
ET	*Esco*	Soil evaporation compensation factor	0	1.0	0.68	0.58
	Gw_Revap	Reevaporation coefficient: this variable controls the amount of water moving from the shallow aquifer to the root zone as a result of soil moisture depletion	0	0.02	0.018	0.018
	Revapmn	Threshold depth of water in shallow aquifer required to allow reevaporation to occur (mm H_2O)	0	100	84.07	84.07
Overland flow	*M_CN2*	Multiplier of moisture condition II curve number	0.4	1.1	0.81	0.81
	Surlag	Surface runoff lag coefficient (day)	0	1.0	0.055	0.055
River routing	*Ch_n2*	Manning's "n" for the main channel	0.01	0.10	0.093	0.052
Infiltration	*M_sol_k*	Multiplier of saturated hydraulic conductivity of soil	0.75	1.20	0.76	0.76
Interflow	*Lat_ttime*	Lateral flow travel time (day)	0	15.0	13.32	13.32
	M_latlyr	Multiplier of lateral flow in soil layer for the day	0	10.0	6.20	9.01
Bedrock percolation	*M_sepday*	Multiplier of percolation into bedrock	0.01	0.15	0.11	0.11
	Rchrg_dp	Aquifer percolation coefficient	0	0.15	0.052	0.052
Groundwater flow	*Alpha_bf*	Base flow recession constant	0	1.0	0.57	0.57
	Gw_delay	Groundwater delay (day)	10	150	38.00	76.65
	Gwqmn	Threshold depth of water in shallow aquifer required before groundwater flow will occur (mm H_2O)	0	100	80.65	80.65
Nitrogen cycle	*M_shallst_n*	Multiplier of nitrate concentration in shallow aquifer	0.9990	0.9999	0.9992	0.9986
	Nperco	Nitrate percolation coefficient	0.25	1.0	0.34	0.50
	Anion_excl	Fraction of porosity from which anions are excluded	0.01	0.60	0.54	0.54
	Dis_stream	Average distance to stream (m)	17.5	27.5	19.90	22.50
	k1	Gas diffusivity (through soil matrix) parameter	10.1			
	M_k	N_2O transfer velocity multiplier for the first-order to fourth-order streams, respectively	3.5, 2.7, 2.6, and 2.5			4.1, 2.7, 2.6, and 2.5
	M_{N_2O}	N_2O concentration multiplier for the first-order to fourth-order streams, respectively	3.4, 2.5, 1.5, and 1.0			

Note. Exp1 is parameter set for SWAT modeling results shown in Figures 1–10, and Exp2 is another parameter set for uncertainty analysis. ET represents evapotranspiration.

Table 2
Properties and Annual Mean Modeled Indirect N_2O Emission Fluxes of Six First-Order Stream Catchments Investigated in the Study

Catchments	Area (km^2)	Dominant land use (%)	Soils (%)	Slope distribution (%)	Annual mean emission fluxes from first-order streams (nmol N_2O m^{-2} s^{-1})	Annual mean emission fluxes from zero-order streams (nmol N_2O m^{-2} s^{-1})
13	1.83	AGRR: 43.92 FRSD: 45.01 RNGE: 7.50	MN234: 100	0–2: 10.57 2–4: 16.21 4–6: 4.58 >6: 68.65	0.011	0.039
34	1.22	AGRR: 73.36 FRSD: 15.15 RNGE: 9.40	MN232: 88.34 MN231: 5.61 MN218: 6.05	0–2: 17.00 2–4: 40.09 4–6: 16.82 >6: 26.09	0.010	0.028
54	1.55	AGRR: 43.29 FRSD: 19.38 HAY: 28.21 RNGE: 7.06	MN232: 83.16 MN218: 16.84	0–2: 11.75 2–4: 20.21 4–6: 7.82 >6: 60.23	0.010	0.041
65	1.35	AGRR: 62.75 FRSD: 20.44 HAY: 11.34	MN232: 53.59 MN218: 46.41	0–2: 11.71 2–4: 30.96 4–6: 17.09 >6: 40.24	0.009	0.033
93	1.58	AGRR: 74.52 Residential: 9.47 RNGE: 9.02 HAY: 6.40	MN230: 97.45 MN234: 2.55	0–2: 10.05 2–4: 62.79 4–6: 25.82 >6: 1.33	0.005	0.016
CC catchment (93.20° W, 44.36° N)	0.22	AGRR: 73.05 Residential: 19.10	MN175: 100	0–2: 15.69 2–4: 14.21 4–6: 15.62 >6: 54.48	0.008	0. 046

Note. Emission fluxes are calculated on the basis of unit catchment area. Locations of five first-order stream catchments within Little Cannon River catchment (LCRC) are shown in Figure 1e, and location of CC catchment is shown in Figure 1b. AGRR—Agricultural Land (row crops); FRSD—Deciduous forest; RNGE—Grasses; HAY—Hay; MN175: Ostrander; MN218: Seaton; MN230: Maxfield; MN231: Frontenac; MN232: Marlean; MN234: Garwin.

1.5 to 2.0 m. According to the U.S. Natural Resources Conservation Service, all soils in LCRC belong to the soil hydrologic group B, which has a moderate infiltration rate and is moderately well-drained to well-drained (Figure 1d). To study the emissions from zero-order streams, five first-order stream catchments with collecting areas of 1.2–1.8 km^2 within the LCRC were randomly selected for modeling; their location information is shown in Table 2 and Figure 1e, and characterization of their land use, soil, and slope is given in Table 2. Our modeling period is from 2002 to 2014.

The mean annual precipitation monitored at the hydrology station (USGS ID: 05355140) near the outlet of LCRC (monitoring location in Figure 1e) during 2011–2014 was 695 mm. Streamflow (Q) and [NO_3^-] were monitored at the same location for the fourth-order Little Cannon River. Q data are available from 1998 to 2010 at daily time steps and at every 15 min since 2011. Stream [NO_3^-] in LCRC was monitored intermittently during March to October from 2007 to 2011. These data sets were obtained from the Minnesota Department of Natural Resources (http://www.dnr.state.mn.us/waters/csg/index.html).

The N_2O emissions from first-order to ninth-order streams were measured in southeastern Minnesota during June to August, 2013 and June to July, 2014. Emissions from five, nine, and seven streams of orders 1, 2–4, and 5–9 were measured in 1 or 2 days, respectively. The number of measurements for each stream in each day ranged from three to fourteen, and the total number of measurements was 43, 39, and 54 for streams of orders 1, 2–4, and 5–9, respectively (Turner et al., 2015). The monitoring locations are shown in the supporting information Figure S1. One of the monitored first-order stream catchments (93.20°W, 44.36°N; Cannon City site, hereafter "CC" catchment) outside the LCRC (Figure 1b) was also used in the present study in order to study the emissions from zero-order streams in its water collecting area. The CC catchment has an area of 0.22 km^2, of which 73% is agricultural land, 19% is residential, 5% is forest, and 3% is rangeland (Table 2 and Figure 2a).

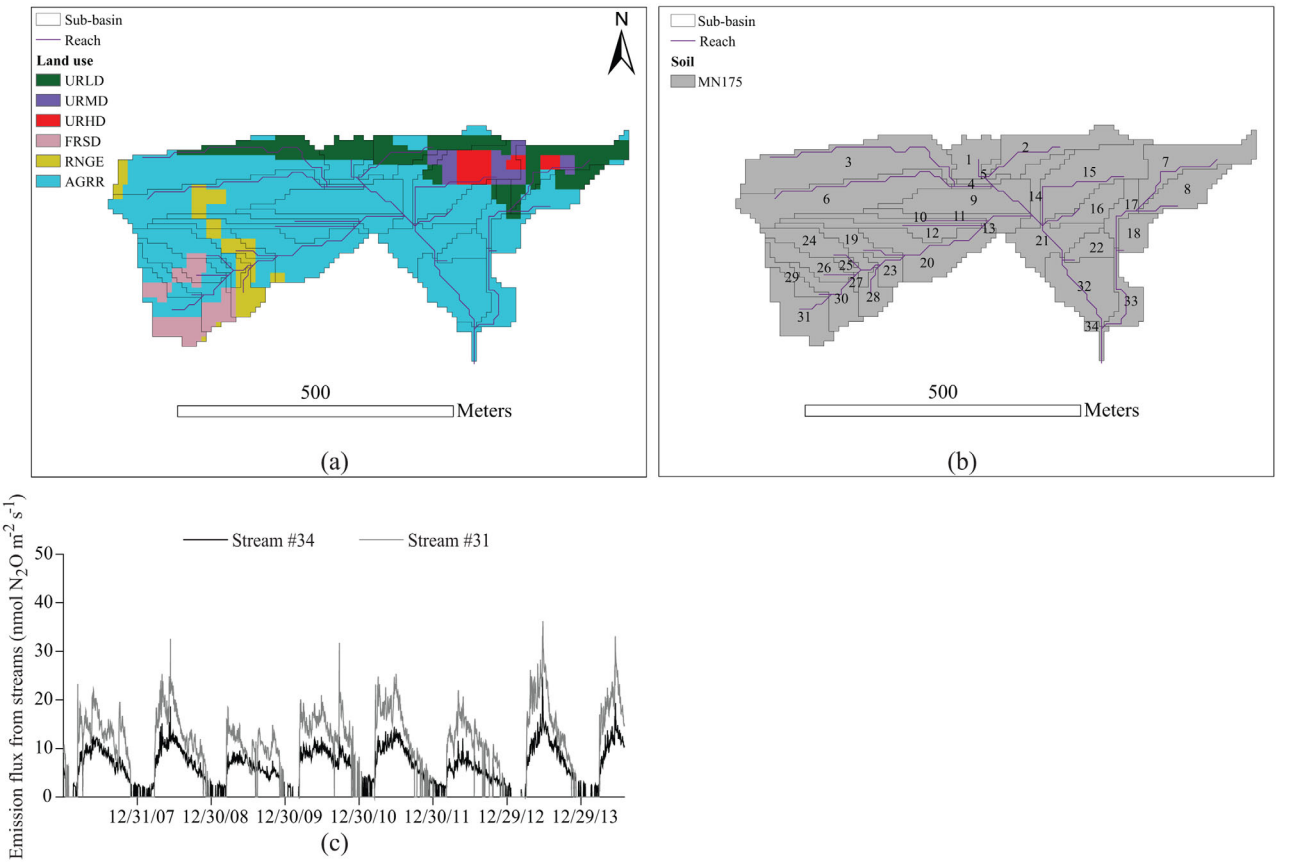

Figure 2. Properties and modeled N_2O emission fluxes from streams in the CC (first-order stream) catchment. Streams #31 and #34 are examples of zero-order and first-order streams, respectively. Location of CC catchment is shown in Figure 1b.

2.2. The SWAT-N_2O Model

SWAT is well suited for the present study for a number of reasons. This model includes descriptions of carbon and N cycles influenced by agricultural management (fertilization, irrigation, crop rotation, growth, harvest). It simulates processes of nitrification and denitrification in the soil, which are a prerequisite for modeling direct N_2O emissions. It also predicts stream [NO_3^-], which is useful for modeling indirect N_2O emissions from streams. Because SWAT is a semidistributed, process-based continuous-in-time model (Arnold et al., 2012), it can predict stream water temperature and provide information on stream hydraulic geometry, both of which are needed for calculating the N_2O gas transfer velocity in streams.

In this study, we have added three modules to SWAT. The first module simulates direct emissions based on the existing soil surface nitrification and denitrification modules. The second module simulates the indirect emissions based on the existing modules for modeling stream [NO_3^-]. The third model is an automatic calibration scheme used to optimize new parameters introduced in the model. This expanded version of the model is referred to as SWAT-N_2O. Specific equations used in these modules are given in the supporting information.

2.2.1. Model Structure of SWAT

SWAT simulates hydrological processes of snowmelt, evapotranspiration, overland flow, infiltration, lateral flow, percolation, groundwater flow, and river routing (Neitsch et al., 2005). Snowmelt is calculated through a temperature-based equation, and overland flow is simulated using the Soil Conservation Service (SCS) curve number method (USDA Soil Conservation Service, 1972) in this study. Precipitation and snowmelt in excess of overland flow are processed as infiltration into the soil profile. Vertical infiltration between two adjacent soil layers is calculated via a storage routing methodology, and lateral flow is calculated by a kinematic storage model. Groundwater flow is simulated using a conceptual linear one-reservoir (shallow aquifer storage) approach.

We have turned off the tile drainage module because of the limited tile drainage area in LCRC (Memorandum of Minnesota Pollution Control Agency (MPCA), 2014; NRI, 1992) and for lack of specific tile drainage information. According to the Minnesota Pollution Control Agency (MPCA, 2014), only 8% of the LCRC is tile-drained. The default SWAT model produced over 80% infiltrated rainwater/snowmelt into the soil profile, which resulted in too much percolation (Fu et al., 2014) into the bedrock for this catchment with comparatively mild terrain. To remediate this deficiency, the lateral flow from soil layers has been amplified with a multiplier (*M_latlyr* in Table 1), and percolation into bedrock has been reduced with a parameter smaller than unity (*M_sepday* in Table 1).

There are three options for modeling the soil carbon and nitrogen cycles in SWAT: static soil carbon (Neitsch et al., 2002), the C-FARM one carbon pool model (Kemanian & Stöckle, 2010), and the Century model (Parton et al., 1994). We chose the Century model option in the present study because this option has a comparatively more complete description of the carbon cycle. Carbon is not simulated with the static soil carbon option. There is only one soil carbon pool in the C-FARM option, while the Century model option includes multiple soil carbon and nitrogen pools, which was added in SWAT by Zhang et al. (2013). The Century model has also been included in the Community Land Model version 4.5 to describe the carbon and nitrogen cycles, including the N_2O emissions from land surfaces (Oleson et al., 2013).

Organic nitrogen and nitrate are transported from land to streams in SWAT (Neitsch et al., 2011). Organic nitrogen is transported with sediment to the stream by surface runoff, and the amount of the transported organic nitrogen is calculated with a function provided by McElroy et al. (1976). Nitrate may be transported to streams via surface runoff, lateral flow, and groundwater flow. SWAT calculates the nitrate concentration in mobile water first, then the amount of nitrate moved with the water is obtained by multiplying the water volume of each pathway and corresponding nitrate concentration (Neitsch et al., 2011).

In SWAT, a catchment is divided into subbasins, and each subbasin is further divided into hydrologic response units (HRUs) each having a unique combination of land use, soil type, and slope. LCRC was divided into 97 subbasins (Figure 1e) and 427 HRUs. The computational time step is daily. The Digital Elevation Model (DEM) was obtained from the National Elevation Dataset with a resolution of one third arc sec (approximately 10 m; https://nationalmap.gov/3DEP/3dep_prodserv.html). Land cover data for the model came from the 2001 National Land Classification Dataset (NLCD), 2011 Edition, amended in 2014 with a resolution of 30 m (Homer et al., 2015; http://www.mrlc.gov/nlcd11_data.php). Soil class data were obtained from the State Soil Geographic Database (STATSGO; US Department of Agriculture-Natural Resource Conservation Service (USDA-NRCS), 1992) distributed with ArcSWAT. Slopes were classified into four categories: 0–2%, 2–4%, 4–6%, and >6%. The meteorological forcing data, including precipitation, wind speed, relative humidity, and solar radiation, were provided by the Climate Forecast System Reanalysis (CFSR) produced by the National Centers for Environmental Prediction (NCEP) (http://globalweather.tamu.edu/).

According to the MPCA (2014), corn-soybean rotation comprises 80% of the crop rotations in the LCRC, continuous corn comprises 10%, and corn-corn-alfalfa- alfalfa-alfalfa rotation represents another 10%. In the present modeling, the corn-soybean rotation is applied to all the agricultural lands for simplicity. In the corn growth phase, we uniformly set the fertilizer date (25 April), beginning date of plant growth (1 May), and harvest date (15 October) (MPCA, 2014). We assumed a fertilizer composition of Urea (46-00-00) (Bierman et al., 2012). All fertilizer was added to the first soil layer in one application at a rate of 350 kg Urea ha^{-1}. In the soybean growth phase, the planting and harvest dates of soybean were 15 May and 10 October in the following year, respectively, and no fertilizer was used (MPCA, 2014).

2.2.2. Emission Module for Soils

The module for the direct N_2O emissions from the soil is based on the SWAT simulation of the nitrification and denitrification processes. Following the calculation in Community Land Model version 4.5, a constant fraction, 6×10^{-4} of the nitrification rate (kg N ha^{-1} day^{-1}; Li et al., 2000), is taken as N_2O emissions. The ratio of N_2 to N_2O from denitrification is a function of CO_2 production in a given soil layer, the NO_3^- concentration in soil water, the gas diffusivity, and soil water content that affects soil anoxic condition. Following the Century approach (del Grosso et al., 2000), the ratio of N_2 to N_2O production by denitrification $P_{N_2:N_2O}$ is

$$P_{N_2:N_2O} = \max\left(0.16k_1, k_1 \times e^{\left(-0.8P_{NO_3:CO_2}\right)}\right) f_{WFPS} \quad (1)$$

where $P_{NO_3:CO_2}$ is ratio of CO_2 production/heterotrophic soil respiration (a proxy of labile C availability that affects denitrification rates in soil) in a given soil layer to the NO_3^- concentration, k_1 is a parameter (affected by soil gas diffusivity) for calibration, and f_{WFPS} is a function of the water-filled pore space (*WFPS*):

$$f_{WFPS} = \max(0.1,\ 0.015 \times WFPS - 0.32) \quad (2)$$

The emission from soils in the Corn Belt calculated with the IPCC bottom-up methodology in Griffis et al. (2013) is around 0.19 nmol N_2O m^{-2} s^{-1}, which is quite close to the EDGAR (Emission Database for Global Atmospheric Research) database value (Figure 3b in their study). We adjusted the soil gas diffusivity parameter k_1 to 10.1 to make the direct emission equal to 0.19 nmol N_2O m^{-2} s^{-1} in our modeling.

2.2.3. Emission Module for Streams

Our module for stream N_2O emissions is based on the SWAT simulation of stream $[NO_3^-]$. The stream N_2O emission is calculated as a function of surface water N_2O concentration, the equilibrium N_2O concentration, and the N_2O transfer velocity,

$$F = k \times ([N_2O\text{–}N_2O_{amb}]) \times 413.2 \quad (3)$$

where F is the emission (nmol N_2O m^{-2} s^{-1}, expressed on the basis of unit water surface area), k is the N_2O transfer velocity (m d^{-1}), $[N_2O]$ and $[N_2O_{amb}]$ are surface water N_2O concentration (mg N_2O-N L^{-1}) and the theoretical N_2O concentration in equilibrium with atmospheric N_2O (mg N_2O-N L^{-1}), respectively. The number 413.2 is a unit conversion factor.

The surface water N_2O concentration $[N_2O]$ is calculated as a function of the simulated stream $[NO_3^-]$ on the basis of the empirical equation established by Turner et al. (2016) for the Upper Mississippi River (UMR; their Figures 4 and equation (5)). UMR is a ninth-order river, and the calculated $[N_2O]$ concentration using their original regression equation is probably too small for the first-order to fourth-order streams in LCRC. For this reason, we added a multiplier (a tuning parameter M_{N_2O}) to the UMR $[N_2O] \sim [NO_3^-]$ equation for the first-order to fourth-order streams in LCRC. In this study, parameter M_{N_2O} was tuned to make the modeled emissions from the first-order to fourth-order streams in LCRC equal to the emissions from corresponding first-order to fourth-order streams reported by Turner et al. (2015) (calibration and validation results shown in section 3.4). The N_2O transfer velocity k is a function of Schmidt number and stream water temperature (Raymond et al., 2012). At a Schmidt number of 600, k is calculated as a function of streamflow velocity, stream slope, depth, discharge, and the Froude number, as shown in Table 2 in Raymond et al. (2012). The k values predicted by Raymond et al.'s (2012) approach are too small in comparison to the transfer velocities reported by Garnier et al. (2009) for the first-order to fourth-order streams in the Seine basin in France. The smaller k values in the present study are caused by the too small water velocity calculated according to the empirical equation (equation shown in Figure 1a in Raymond et al., 2012). In our study, we multiplied the k value from Raymond et al.'s (2012) approach with a factor M_k.

The zero-order streams in the five first-order stream catchments in LCRC and the CC catchment used the same M_k and M_{N_2O} as the first-order streams in the LCRC. The equilibrium N_2O concentration $[N_2O_{amb}]$ was calculated using equations (2), (4), and (5) in Sander (1999) as a function of air temperature, atmospheric N_2O concentration, and the Henry's law constant. When the difference between $[N_2O]$ and $[N_2O_{amb}]$ was small ($0.8 < [N_2O] \div [N_2O_{amb}] < 1.2$), the stream emissions were set to zero, following Beaulieu et al. (2015) and Turner et al. (2016).

2.2.4. Model Parameter Optimization

The calibration was made in the sequence of Q, $[NO_3^-]$, and N_2O emission. A total of 24 parameters in SWAT-N_2O were optimized against field data on Q and $[NO_3^-]$ (Table 1). The parameter selection and corresponding ranges were based on the studies of Zhang et al. (2008) and Fu et al. (2014, 2015). Because SWAT-N_2O involves new parameters, the default SWAT calibration module (SWAT-CUP) is no longer appropriate. Instead, we replaced SWAT-CUP with a Monte Carlo module to calibrate the model and optimize the parameter set. A total of 40,000 parameter sets were used for the model calibration (supporting information Figures S2 and S3).

The streamflow data were split into three periods, with the first period (2002–2006) used for model spin-up, the second period (2007, 2010, and 2011; flow data missing in 2008 and data were poorly archived in 2009) for model calibration, and the third period (2012–2014) for model validation. The stream $[NO_3^-]$ data were split into two periods, with the first period (2007–2008) used for model calibration, and the second period (2009–2011) for model validation.

We used the Nash-Sutcliffe efficiency (NSE; Nash & Sutcliffe, 1970) to do automatic calibration and validation for Q and $[NO_3^-]$. NSE, a widely used criterion to judge model accuracy in hydrology modeling studies, is calculated as:

$$NSE = 1 - \frac{\sum_{i=1}^{n} (O_i - S_i)^2}{\sum_{i=1}^{n} (O_i - \bar{O})^2} \quad (4)$$

where n is number of observations, O and S represent observation and simulated values, respectively, and $\bar{O}$ is the average of O. An NSE value of one represents a perfect fit between the simulation and the observation. After the parameter sets with acceptable NSEs for both Q and $[NO_3^-]$ were obtained, the coefficient of determination R^2, as well as the Percent BIAS (PBIAS; Gupta et al., 1999), were used to further evaluate the modeling results. *PBIAS* is calculated as:

$$PBIAS = \left[\frac{\sum_{i=1}^{n} (O_i - S_i) * 100}{\sum_{i=1}^{n} O_i} \right] \quad (5)$$

The optimized parameter set from the Monte Carlo calibration (Exp2 in Table 1) still did not perform very well for $[NO_3^-]$, so we did further calibrations on the basis of the optimized parameter set "Exp2." Specifically, further simulations were done with one parameter of "Exp2" ranging from its bottom boundary to its top boundary, while all other parameters of "Exp2" were fixed. Such simulations looped through all parameters, and as a result, a new parameter set "Exp2-1" with better performance (higher accuracy) than "Exp2" was obtained. Another round of simulations were done based on parameter set "Exp2-1," and so on. The simulations were stopped when the model accuracy (NSE) was not clearly improved from the previous round of simulations. The final parameter set "Exp1" (Table 1) was then used for the subsequent modeling analysis.

After the model parameters were optimized for Q and $[NO_3^-]$, additional calibration was carried out on direct soil N_2O emissions and indirect stream N_2O emissions. The multipliers in the k equation and the $[N_2O]$ equation (M_k and M_{N_2O} in supporting information Text S1, respectively) were adjusted to force agreement between the modeled stream N_2O flux and the N_2O flux observed by Turner et al. (2015) for first-order to fourth-order streams. For first-order streams, data in June, 2013 were used to calibrate the model, and data in the other three periods (July, August of 2013, and June of 2014) were used for validation. Specifically, the mean N_2O emission of all first-order streams was adjusted to fit Turner et al.'s (2015) observation in June, 2013, then modeling results in the other three periods were compared with their observations for validation. For second to fourth-order streams, all observed data were used for calibration due to the limited data availability. The parameter used to describe denitrification in soils (k_1) was calibrated against the direct emissions observed for corn and soybean crops and natural soils (Griffis et al., 2013).

3. Results

In this section, we show the identifiable parameters, analyze the sensitivity of modeled $[NO_3^-]$ to various parameters, and assess the model accuracy by comparing the simulated Q and stream $[NO_3^-]$ with observations. We then investigate the relationships between river collecting area and modeled stream $[NO_3^-]$. After that, we present modeled N_2O emissions, and examine hot moments and hot spots. Modeled $[NO_3^-]$ was directly compared with observed $[NO_3^-] + [NO_2^-]$ in this study, because stream $[NO_2^-]$ is quite small compared with $[NO_3^-]$, e.g., the modeled mean annual $[NO_2^-]$ was only 1% of the modeled $[NO_3^-]$ in this study.

3.1. Identifiable Parameters and Sensitivity Analysis for Nitrate Concentration

A total of 40,000 parameter sets were used for the model calibration and validation, and the ranges of these parameters are shown in Table 1. The maximum NSEs for calibration and validation of daily Q ($[NO_3^-]$) were 0.56 (0.51) and 0.68 (0.33), respectively. In this study, identifiable parameters were qualitatively judged from their dotty figures: the more concentrated the pattern of dots was near the upper envelope of the NSE values, the more identifiable the parameter was (Fu et al., 2015). Each parameter set was composed of 24 parameters, and the x axis and y axis of each panel of the dotty plot corresponded to the value of each parameter and the NSE value calculated using the parameter, respectively. According to the dotty plots of NSE for Q (supporting information Figure S2), four parameters are comparatively identifiable in the Q modeling. They are (1) a snow pack temperature lag factor (*Timp*), which is used in predicting snowmelt

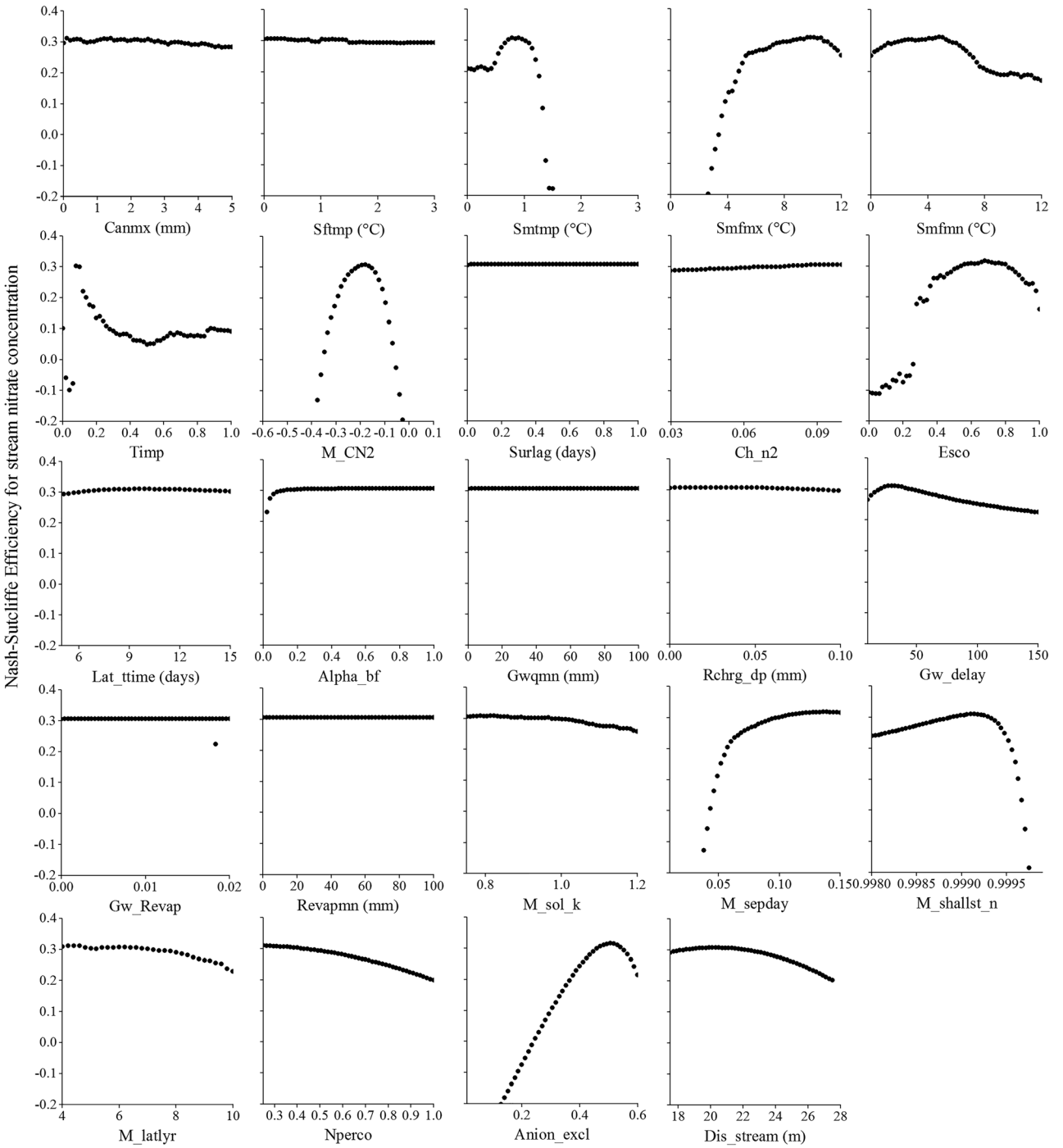

Figure 3. Sensitivity of Nash-Sutcliffe efficiency of stream nitrate concentration to parameters. The meanings of parameters are shown in Table 1.

timing and rate, (2) a multiplier of moisture condition II curve number (*M_CN2*), which determines the amount of overland flow, (3) a soil evaporation compensation factor (*Esco*), which controls the maximum evaporation for a specific soil depth, and (4) a multiplier of percolation into bedrock, which controls percolation into bedrock (*M_sepday*). For the [NO_3^-] modeling (supporting information Figure S3), *M_CN2* and *Esco* are identifiable parameters. Five parameters that determine the [NO_3^-] loss in lateral flow and groundwater flow during the flow convergence processes, including multiplier of lateral flow in soil layer for the day (*M_latlyr*), fraction of porosity from which anions are excluded (*Anion_excl*), average distance to stream

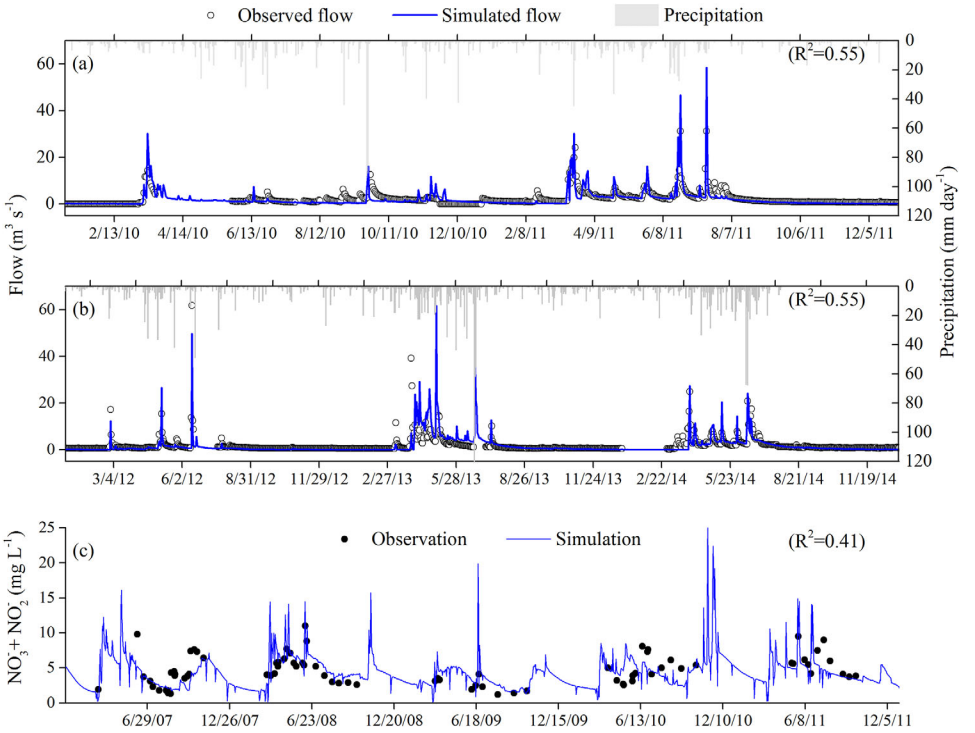

Figure 4. (a and b) Observed and simulated streamflow and (c) sum of nitrite and nitrate near the outlet of the Little Cannon River Catchment. (a) Calibration period; (b) validation period.

(*Dis_stream*), multiplier of percolation into bedrock (*M_sepday*), and multiplier of nitrate concentration in the shallow aquifer (*M_shallst_n*), are also identifiable.

Because stream N_2O emissions were assumed to be influenced by stream [N_2O] and [NO_3^-], a sensitivity analysis of the modeled [NO_3^-] to various parameters was performed on the basis of the parameter set Exp1 shown in Table 1. Specifically, simulations were made by increasing one parameter linearly from its minimum value to its maximum value (Table 1) and keeping other parameters fixed. The results show that the stream [NO_3^-] is extremely sensitive to snow melt base temperature (*Smtmp*), maximum snowmelt factor for 21 June (*Smfmx*), *Timp*, *M_CN2*, *Esco*, *M_sepday*, *M_shallst_n*, and *Anion_excl*, and is also sensitive to maximum snowmelt factor for 21 December (*Smfmn*), groundwater delay (*Gw_delay*), multiplier of saturated hydraulic conductivity of soil (*M_sol_k*), *M_latlyr*, nitrate percolation coefficient (*Nperco*), and *Dis_stream*. The sensitive parameters have to be calibrated in modeling stream [NO_3^-] and [N_2O] (Figure 3).

3.2. Modeling of Streamflow and Nitrate Concentration

Accurate modeling of *Q* and stream [NO_3^-] is prerequisites for simulation of stream N_2O emissions. We selected one parameter set with comparatively good results (NSE, R^2, and PBIAS) for both *Q* and [NO_3^-] to run the model and investigate the stream N_2O emissions (Table 1). The daily (monthly) NSE was 0.31 (0.44) and 0.41 (0.62) for *Q* during the calibration and validation periods, respectively, and the corresponding value for the whole period was 0.37 (0.55). The daily (monthly) NSE was 0.46 (0.49) and 0.10 (0.36) for the stream [NO_3^-] during the calibration and validation periods, respectively, and the corresponding value for the whole period was 0.32 (0.42). The R^2 between simulated and observed *Q* including both the calibration and validation periods for a daily (monthly) time step was 0.55 (0.74), and corresponding value for stream [NO_3^-] was 0.41 (0.48). The mean observed and simulated *Q* at the outlet of LCRC during 2007–2014 was 2.03 $m^3\ s^{-1}$ (calibration period: 2.27 $m^3\ s^{-1}$; validation period: 1.81 $m^3\ s^{-1}$) and 1.80 $m^3\ s^{-1}$ (calibration period: 1.93 $m^3\ s^{-1}$; validation period: 1.68 $m^3\ s^{-1}$), respectively, corresponding to a PBIAS of 11%. The mean observed and simulated stream [NO_3^-] during 2007–2011 was 4.60 mg NO_3-N L^{-1} (calibration period: 4.63 mg NO_3-N L^{-1}; validation period: 4.56 mg NO_3-N L^{-1}) and 4.27 mg NO_3-N L^{-1} (calibration period: 4.24 mg NO_3-N L^{-1}; validation period: 4.32 mg NO_3-N L^{-1}), respectively, corresponding to a PBIAS of 7%. All the results that follow were obtained using the parameter set Exp1.

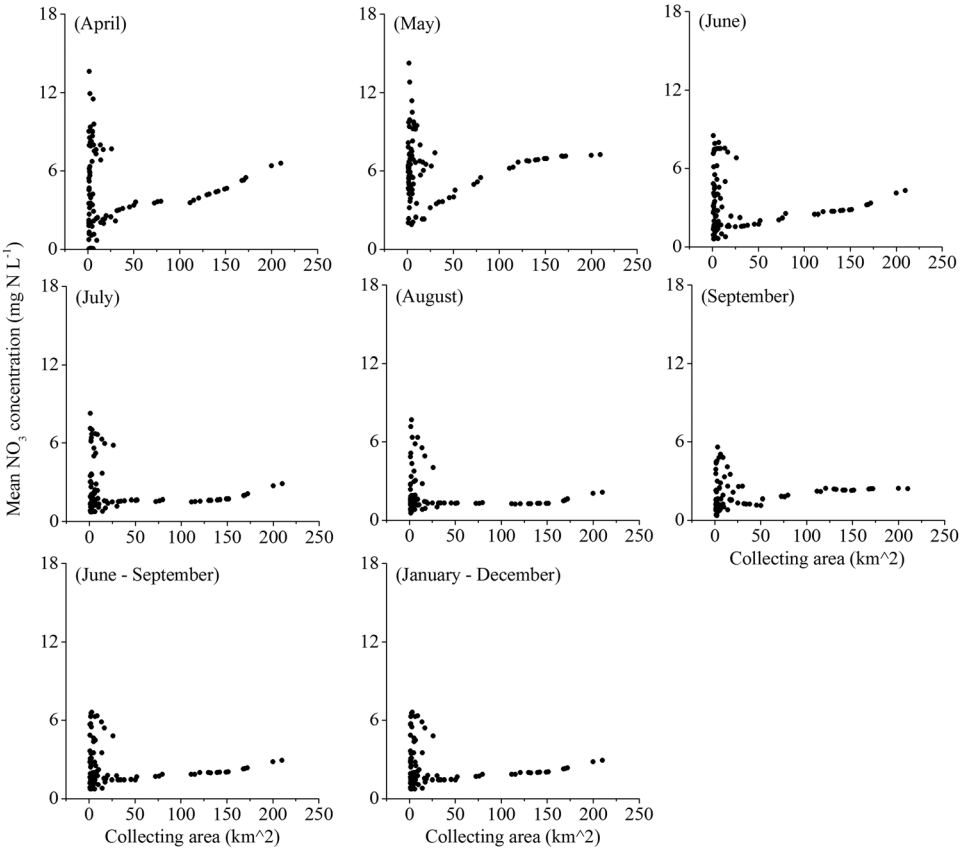

Figure 5. Correlations between river collecting area and mean modeled stream nitrate concentration for different months during 2007 and 2014. Each dot represents a stream.

A NSE $\geq$ 0.50 (0.50), an absolute PBIAS $\leq$ 25% (70%) (Moriasi et al., 2007), and an $R^2 \geq 0.50$ (0.50) (Parajuli et al., 2009) are widely used standards for satisfactory model accuracy for *Q* (stream $[NO_3^-]$) for a monthly time step. Previous SWAT study for the Little Cannon River catchment (MPCA, 2014) established the satisfactory accuracy for monthly *Q* (stream $[NO_3^-]$) as NSE $\geq$ 0.25 (0.25), $R^2 \geq 0.25$ (0.25), and absolute PBIAS $\leq$ 25% (70%). The modeling for monthly *Q* (stream $[NO_3^-]$) for the whole modeling period of 2007–2014 (2007–2011) in the present study resulted in a NSE of 0.55 (0.42), an R^2 of 0.74 (0.48), and an absolute PBIAS of 11% (7%). Therefore, the simulation accuracy in present study complies with the MPCA (2014) satisfactory ratings, and is close to the widely used satisfactory model accuracy (Moriasi et al., 2007; Parajuli et al., 2009).

Comparisons between the simulated and the observed *Q* and $[NO_3^-]$ time series are shown in Figure 4. The simulated *Q* fitted very well with the observed temporal variations (Figures 4a and 4b), and the simulated stream $[NO_3^-]$ also captured the observed seasonal dynamics reasonably well. Large increases in $[NO_3^-]$ in April and May, seen in both the observed and the simulated time series, reflected the combined influence of fertilization (28 April) and strong leaching caused by the snowmelt in April and high rainfall intensity in May (Figures 4a and 4b). During the winter, the nonzero *Q* and $[NO_3^-]$ (Figure 4c) might have been caused by the groundwater flow because there was no overland flow at temperatures below 0°C.

3.3. River Collecting Area Versus Modeled Stream Nitrate Concentration

The correlation between river collecting area and modeled multiyear average stream $[NO_3^-]$ during 2007–2014 is shown in Figure 5. The modeled multiyear average $[NO_3^-]$ of streams with small collecting areas varied in a large range. For example, the May value varied from 2 to 14 mg NO_3-N L^{-1} for collecting areas smaller than 5 km^2. The large variability was attributed to variable soil hydraulic conductivity and therefore the resulting percolation of $[NO_3^-]$ into bedrock (supporting information Figure S4). $[NO_3^-]$ was less variable for streams with the collecting area larger than 50 km^2, because larger streams may be more controlled by regional groundwater. The increase of $[NO_3^-]$ with collecting area beyond 20–25 km^2 was attributed to the

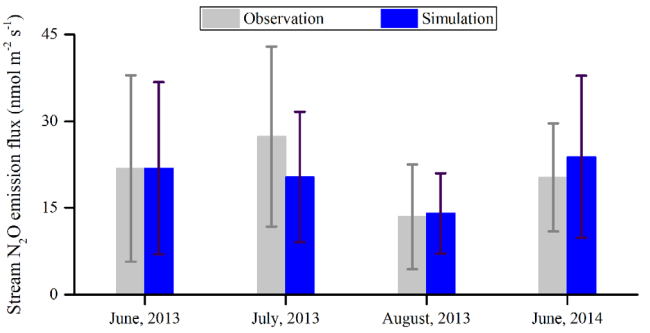

Figure 6. Model calibration and validation for indirect N_2O emission flux from first-order streams. Observed emission flux is the average of different monitoring sites for a specific monitoring day, and the simulated flux is the average for all first-order streams during 2 weeks around a specific monitoring day. Vertical lines represent one standard deviation.

mixture of low-[NO_3^-] flow from the main stream and high-[NO_3^-] inflow from first-order streams (Figures 1e and 5).

The low [NO_3^-] values for streams with small collecting areas in Figure 5 was attributed to small leaching of nitrate into streams (supporting information Figure S4a). Specifically, the low [NO_3^-] mainly occurred in drainage areas containing soil type Seaton (MN218; Figure 1d), which has small saturated hydraulic conductivity (1.0–2.7 mm h^{-1}) and for this reason, nitrate cannot drain easily into the streams (supporting information Figure S4b), resulting in large ratio of nitrate percolation into bedrock to nitrate input into streams.

3.4. Calibration and Validation for Stream N_2O Emissions

The multiplier M_{N_2O}, which tunes the UMR [N_2O] ~ [NO_3^-] equation, was tuned to be 3.4, 2.5, 1.5, and 1.0 for the first-order to fourth-order streams in LCRC after calibration, respectively (Table 2). The modeled [N_2O] after adjustments were still within the range of 1–4 μg N L^{-1} observed by Garnier et al. (2009) in the Seine drainage network in France. The multiplier to the *k* value from Raymond et al. (2012) (M_k) was 3.5, 2.7, 2.6, and 2.5 for the first-order to fourth-order streams, respectively. After the adjustment, the *k* value was still within the ranges of 5.04–8.88, 3.84–6.72, 2.88–5.04, and 2.16–3.60 m d^{-1} observed from the first-order to fourth-order streams in the Seine basin in France, respectively (Garnier et al., 2009).

As described in method section 2.2.4, the modeled N_2O emissions were adjusted to fit the observations in June 2013. The modeling results were then compared with the observations in the other three periods. The simulated emission was 25.5% smaller than the observation in July 2013, and was 4.5% and 17.6% larger than the observation in August 2013 and June 2014, respectively (Figure 6). Overall, model accuracy with a maximum difference of 25.5% (PBIAS = 25.5%) between observation and simulation appeared acceptable (Moriasi et al., 2007), and the seasonal dynamics of the observed emissions, i.e., larger emissions in June and July and smaller emissions in August, were also reproduced by the model.

3.5. Importance of Indirect Emissions

The first-order to fourth-order streams occupy only 0.33% of the total area of the LCRC. The modeled multi-year average indirect stream emissions from these streams varied from 0.65 nmol N_2O m^{-2} s^{-1} (a fourth-order stream) to 20.19 nmol N_2O m^{-2} s^{-1} (a first-order stream) with an average of 6.13 nmol N_2O m^{-2} s^{-1} (Figure 7a). Specifically, the mean modeled indirect emission was 9.11 ± 4.50, 5.63 ± 1.81, 2.47 ± 0.63, and 1.24 ± 0.36 (mean ± 1 standard deviation) nmol N_2O m^{-2} s^{-1} for first-order, second-order, third-order, and fourth-order streams in the LCRC, respectively. The mean modeled emission from first-order to fourth-order order streams during June–August was 12.19 nmol N_2O m^{-2} s^{-1}, which almost doubled the annual average value (6.13 nmol N_2O m^{-2} s^{-1}). These fluxes were expressed on the basis of unit stream surface area. The corresponding numbers of streams used for calculating the mean and standard deviation of the stream flux were 49, 16, 15, and 17. The mean emission from the first-order to fourth-order streams in the LCRC was 0.018 nmol N_2O m^{-2} s^{-1} on the basis of unit catchment area. For comparison, the direct soil emission is on average 0.19 nmol N_2O m^{-2} s^{-1} on the basis of unit catchment area. Therefore, the total indirect emissions from first to fourth-order streams were roughly 10% of the direct N_2O emissions to the atmosphere from the LCRC.

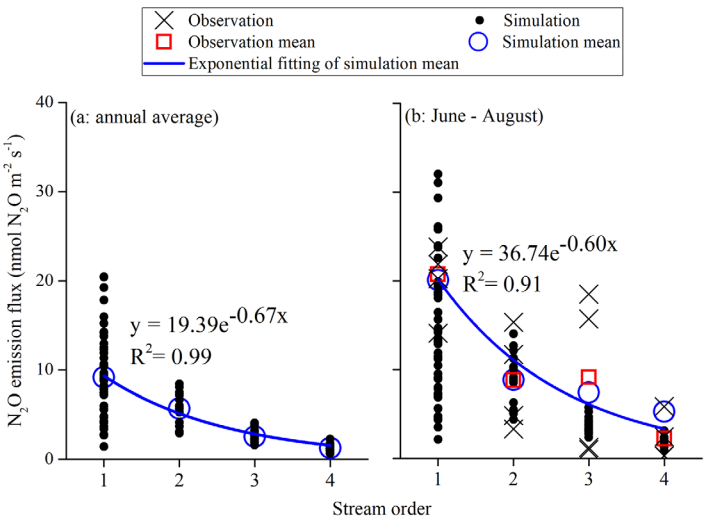

Figure 7. Indirect N_2O emission fluxes from streams of different orders compared with observation. Observations are conducted during June–August, 2013 and June–July, 2014 in plot (b). Emission fluxes are expressed on the basis of unit water surface area.

As for the six first-order stream catchments (five in LCRC and one in CC), the mean annual emissions from zero-order streams were 10.84 ± 6.78, 6.21 ± 7.44, 9.71 ± 5.21, 8.51 ± 6.10, 4.17 ± 2.31, and

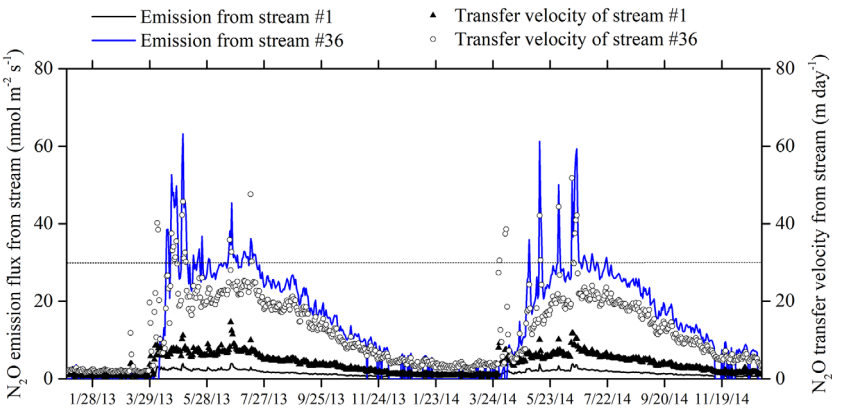

Figure 8. Modeled N_2O emission fluxes and transfer velocities of streams. Streams #1 and # 36 are examples of the fourth-order and first-order streams, respectively. Locations of these two streams are shown in Figure 1e.

5.20 ± 3.17 (mean ± 1 standard deviation) nmol N_2O m^{-2} s^{-1} in catchments 13, 34, 54, 65, 93, and CC, respectively (Table 2), and corresponding values for June–August were 20.86 ± 12.92, 11.51 ± 13.87, 17.26 ± 9.31, 16.21 ± 11.63, 8.42 ± 4.33, and 12.33 ± 7.06 nmol N_2O m^{-2} s^{-1} (Table 2 and Figure 2c). There were 99 (out of 109 total streams), 69 (out of 71 total streams), 80 (out of 88 total streams), 65 (out of 73 total streams), 78 (out of 84 total streams), and 30 (out of 34 total streams) zero-order streams in catchments 13, 34, 54, 65, 93, and CC, respectively. The surface areas of these zero-order streams occupied 0.22–0.40% of the corresponding catchment area, with an average value of 0.25%. Expressed on the basis of unit catchment area, the emissions from zero-order streams were in the range of 0.016–0.046 nmol N_2O m^{-2} s^{-1}, with an average of 0.034 nmol N_2O m^{-2} s^{-1} (Table 2). For comparison, the average emission from the first-order streams in these six first-order stream catchments varied from 0.005 to 0.011 nmol N_2O m^{-2} s^{-1} on the basis of unit catchment area, with an average of 0.0088 nmol N_2O m^{-2} s^{-1}, which was close to mean value of all the first-order streams in LCRC (0.011 nmol N_2O m^{-2} s^{-1}).

Overall, the modeled multiyear average indirect emissions from the zero-order streams, indirect emissions from the first-order to fourth-order streams, and direct emissions from land surface in the LCRC were 0.034, 0.018, and 0.19 nmol N_2O m^{-2} s^{-1}, on the basis of unit catchment area, contributing 14%, 7%, and 79% to the total emissions, respectively.

3.6. Hot Moments in Indirect Emissions

Emission hot moments, or rapid temporal increases in the N_2O flux, were evident in the modeled data on the stream N_2O flux. Figure 8 presents two examples, one for a fourth-order stream (stream 1 with annual indirect emission 1.16 nmol N_2O m^{-2} s^{-1} on the basis of unit stream surface area) and the other for a first-order stream (stream 36 with annual indirect emission 13.07 nmol N_2O m^{-2} s^{-1} on the basis of unit stream surface area). These hot moments generally coincided with sudden increases of the modeled gas transfer velocity, and the sudden increases of the modeled gas transfer velocity were caused by rapid increase in flow velocity (supporting information Text S1), which were induced by the snowmelt and heavy precipitation events. The steeper river slope is the reason for the larger modeled gas transfer velocity of stream 36 (slope 1.91%) than stream 1 (slope 0.12%). If we use a threshold of 30.0 nmol N_2O m^{-2} s^{-1} on the basis of unit stream area to define hot moments for stream #36, the total emissions during hot moments contributed 54% and 37% to the total annual emissions during 2013 and 2014, respectively. The total durations of these hot moments were only 13% and 7% during 2013 and 2014, respectively. Omitting these hot moments, as in some field experiments with infrequent measurements, would cause serious low biases in the annual flux.

3.7. Hot Spots in Direct Emissions

The spatial distributions of the direct emissions from soils and the indirect emissions from streams are shown in Figure 1e. Clear spatial patterns can be identified for both. The southwest and northeast subbasins show high (>1 nmol N_2O m^{-2} s^{-1}) and low (<0.010 nmol N_2O m^{-2} s^{-1}) direct emissions, respectively. Here the flux values are expressed on the basis of unit ground surface area. The northeast subbasins are covered

by three well-drained soils, Estherville (MN229), Frontenac (MN231), and Marlean (MN232) (Figure 1d), which have high saturated hydraulic conductivity (39.0–550.0, 4.4–26.0, and 4.8–25.0 mm h^{-1}, respectively). Anaerobic conditions rarely occurred in these soils. In contrast, the soil type in the southwest subbasins is mainly Maxfield (MN230) with low saturated hydraulic conductivity of 1.1–5.5 mm h^{-1}, implying frequent occurrence of anaerobic conditions. Frequent occurrence of anaerobic conditions corresponds to frequent occurrence of denitrification and more N_2O emissions. Some of the subbasins in the southwest portion of the model domain were emission hot spots. Given a hot spot threshold 90% percentile, these hot spots occupy only 13.9% of the total catchment, but they contributed 86.8% to the direct emissions in LCRC.

4. Discussion

4.1. Exponential Decline of Indirect Emission With Increasing Stream Order

Although some streams can act as sinks of N_2O (Soued et al., 2016), field studies for agricultural areas showed that most streams are generally supersaturated with respect to atmospheric N_2O (Garnier et al., 2009; Turner et al., 2015, 2016). Turner et al. (2015) reported that the stream emission decreases exponentially with increasing stream order in southeastern Minnesota. According to Turner et al. (2015), the exponential pattern is assumed to be caused by smaller stream [N_2O] and lower gas transfer velocities in higher-order streams. Turner et al. (2015) reported that nitrogen is transformed and removed rapidly via nitrification and denitrification in headwater steams, resulting in high N_2O production potential and [N_2O] there, but the N_2O production potential declines rapidly as stream order increases, because the first-order rate of nitrogen loss within streams can decline by as much as 90% down the stream order (Alexander et al., 2000). Garnier et al. (2009) found a similar pattern in the Seine Basin in Europe. First-order streams are hot spots for N_2O emissions in the Seine Basin due to receiving water from tile drainage and groundwater seepage with high N_2O concentration. Stream [N_2O] is very high at groundwater spring and tile drainage outlets (2.8–4.1 μg N L^{-1}) but decreases rapidly to about 1 μg N L^{-1} at a distance of 50 m from the outlets (Garnier et al., 2009). Rapid decreases in stream [N_2O] and N_2O emissions with distance downstream from an agricultural pipe outlet were also reported for an UK experimental site by Reay et al. (2003).

In the present study, the mean modeled stream flux in the summer (June–August) decreases exponentially with stream order (Figure 7b), a pattern that was consistent with the observation reported by Turner et al. (2015). Figure 10 illustrates that the stream [NO_3^-] does have influences on the stream [N_2O] and subsequently on the exponential decline of N_2O emission with stream order. Figure 8 shows the influences of the gas transfer velocity on the N_2O emissions: higher-order streams have smaller gas transfer velocities and smaller N_2O emissions. Furthermore, the emission hot moments are also caused by high gas transfer velocity, as shown in Figure 8.

In the field observations of Turner et al. (2015), the greatest variability of stream N_2O flux occurred in first-order streams, and higher-order streams showed more stable fluxes. This variability pattern is confirmed by the present modeling study (Figures 7b). There are some comparatively smaller N_2O emissions from first-order streams (e.g., denoted by dots below blue circles in Figure 7), and the modeling results illustrated that these smaller fluxes might be caused by two main mechanisms: (a) larger denitrification rates of the land surface in the subcatchment containing the stream (Figure 9) that reduced nitrate availability and leaching into the stream, and (b) the larger ratio of nitrate percolation into bedrock to nitrate leaching that also reduced nitrate availability and leaching into the stream via lateral flow (supporting information Figure S4). These two mechanisms work together, resulting in smaller stream [NO_3^-] and subsequently smaller N_2O emissions from some first-order streams.

4.2. Magnitude of the Indirect Emissions

Turner et al. (2015) reported that the IPCC inventory methodology yields a flux 0.012 nmol N_2O m^{-2} s^{-1} for streams in southern Minnesota, or about 5% of the total N_2O emissions from southern Minnesota to the atmosphere. For comparison, the mean stream flux extrapolated from their stream observations is much higher, at 0.125 nmol N_2O m^{-2} s^{-1} on the basis of unit catchment area, representing 35% of the total emissions. In the study of Garnier et al. (2009), indirect emissions from streams based on observed [N_2O] and calculated gas transfer velocity accounts for about 1.4% of the total emissions in the Seine Basin, while the corresponding proportion with the IPCC methodology is 9.7%. Garnier et al. (2009) attributed the difference between the observation method (1.4%) and the IPCC methodology (9.7%) to omission of emissions from

riparian zones. More recently, Grossel et al. (2016) reported that the indirect emissions measured from streams in an agricultural landscape (winter wheat and barley) with tile drainage in central France contributed only 1.6% to the total site emissions. The large differences in the indirect emissions between the study by Turner et al. (2015) and those by Garnier et al. (2009) and Grossel et al. (2016) can be partially explained by different observation periods: In Turner et al. (2015), the observations were obtained in high emission months (June and August), while in Garnier et al. (2009) and Grossel et al. (2016), the experiments covered a full year. According to Figure 7, the stream N_2O emissions during June–August is 65% greater than the mean annual value.

Zero-order streams in the Corn Belt were suspected to be emission hot spots (Turner et al., 2015). In the present study, on the basis of unit catchment area, the mean annual emissions from zero-order streams may contribute 0.034 nmol N_2O m^{-2} s^{-1} to the total emissions, and emissions from zero-order streams are 3.9 times of those from the first-order streams (0.0088 nmol N_2O m^{-2} s^{-1}). If we extrapolate the emissions from first-order to fourth-order streams to zero-order streams using the exponential equation in Figure 7a, the mean annual emission from zero-order streams is approximately doubled, at 0.066 nmol N_2O m^{-2} s^{-1}. Under such circumstances, the sum of emissions from zero (0.066 nmol N_2O m^{-2} s^{-1}) and first (0.011 nmol N_2O m^{-2} s^{-1}) order streams represents 41% of the direct emissions, and could reconcile the disparity between top-down and bottom-up budget estimates (0.11 nmol N_2O m^{-2} s^{-1}; Turner et al., 2015), and the direct and total indirect emissions are 0.19 and 0.082 nmol N_2O m^{-2} s^{-1}, respectively. As described above, the IPCC inventory methodology yields a flux 0.0125 nmol N_2O m^{-2} s^{-1} for streams in southern Minnesota (Turner et al., 2015). The findings in the present study imply that the IPCC N_2O emission factor for streams in Corn Belt should be increased by 3.2 ((0.034 + 0.018) ÷ 0.0125 – 1) times if we use the mean flux modeled for the six zero-order streams or by 5.7 ((0.066 + 0.018) ÷ 0.0125 – 1) times if the mean flux of the zero-order streams is extrapolated from the exponential regression fit shown in Figure 7a. Because the observed [N_2O] decreased exponentially (quickly) downstream from springs or agricultural tile-drain outlets (Garnier et al., 2009; Reay et al., 2003), illustrating higher [N_2O] in zero-order streams than first-order ones, it seems appropriate, therefore, to calculate the emissions from zero-order streams using emission parameters for first-order streams for the lower boundary (i.e., 3.2 times).

It is likely that the true flux of the zero-order streams falls between the above two estimates. In our model calculation for the zero-order streams in the six first-order stream catchments, we assumed that the stream N_2O emissions occur only when streamflow is larger than 1×10^{-4} m^3 s^{-1}. It is possible that stream N_2O emissions occur even under conditions of low streamflow. Previous studies have demonstrated that riparian zones are potentially significant sources of N_2O emissions (Billen et al., 2009; Skiba & Ball, 2002; Thieu et al., 2009). Garnier et al. (2009) concluded that the indirect emissions can contribute 13–17% to the total emissions of the Seine Basin if the riparian zones are considered. The intermittent zero-order streams can also behave like riparian zones under low flow conditions. Additional field studies are needed to elucidate these mechanisms.

4.3. Correlation Between Direct and Indirect Emissions

The spatial relationships between direct and indirect emissions deserve some attention. Grossel et al. (2016) monitored the direct N_2O emissions from tile-drained and undrained experimental plots and intermittent streams, and reported that the direct N_2O emissions from the drained plots are 10-fold smaller than those from the undrained plots, because the undrained plots are frequently saturated and denitrification occurs more frequently. They also reported that the decrease of the direct N_2O emissions due to drainage can be partially counteracted by an increase in the indirect N_2O emissions. The simulation results in the present study also predict that a negative correlation exists, to some extent, between the direct and the indirect emissions in the LCRC (Figure 9). The indirect flux from first-order stream catchments is negatively correlated with the direct soil flux in the corresponding catchments ($R^2 = 0.12$, number of catchments = 49, $p < 0.02$; Figures 1e and 9a). The negative correlation can be explained by the fact that land soils with small saturated hydraulic conductivity resulted in (a) less nitrate leaching to the stream and subsequently lower stream N_2O emissions and (b) more nitrate in the soil converted by denitrification to N_2 and N_2O. Figure 9b excludes the influence of high nitrate percolation into bedrock and less nitrate leaching that results in small N_2O emissions from some first-order streams. If these first-order streams with small emissions are excluded in Figure 9b, a stronger negative correlation is found between direct and indirect emissions ($R^2 = 0.63$, $p < 0.05$).

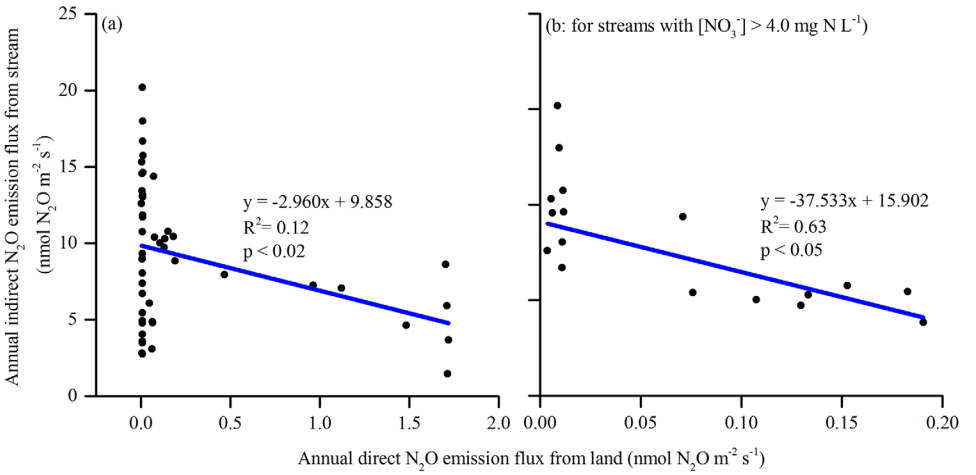

Figure 9. Correlations between modeled direct and indirect emission fluxes. Data shown in this figure are for first-order streams. Plots (b) are parts of results shown in plot (a).

Land surface N_2O emissions are affected by soil texture and slope. Compared with other soil textures in the LCRC, the Maxfield soil (MN230) in southwestern subbasins has larger percentages of clay (23.0–32.0%) and silt (43.9–63.5%) and smaller slope. The soil water-filled pore space (WFPS), covered by Maxfield soil with a small hydraulic conductivity (K_{sat}: 1.1–5.5 mm h^{-1}), was frequently above the threshold for the occurrence of denitrification, and subsequently direct emissions. Several published studies also reported that N_2O emissions increase with clay content and decrease with sand content (Gaillard et al., 2016; Skiba & Ball, 2002), although some studies (e.g., Gu et al., 2013) found the N_2O emissions increase with the silt content and decrease with the clay content.

Annual precipitation and streamflow have increased in the Corn Belt over the past 50 years (Baker et al., 2012). The findings in the present study imply that the direct emissions from the soil may have increased due to enhanced frequencies of anoxic conditions and denitrification, and that indirect emissions may have also increased due to more leaching of nitrate into streams and the enhanced gas transfer velocity responding to the increased streamflow velocity. To reduce flood risks and nutrient pollutants, restored wetlands and ponds are recommended for the Cannon River Watershed (Memorandum of Minnesota Pollution Control Agency (MPCA), 2015). It is not known whether these wetlands or ponds may become N_2O emission hot spots like drainage ditches and zero-order streams, and Best Management Practices (BMPs) that reduce nitrate leaching losses through increasing denitrification may also increase N_2O emissions (Mulla et al., 2005).

4.4. Linear Relationship Between $[NO_3^-]$:$[N_2O]$ on the Annual Scale

The IPCC (2006) method (De Klein et al., 2006) for estimating the indirect emission factor predicts a linear relationship between $[NO_3^-]$ and $[N_2O]$ on the annual scale (Hama-Aziz et al., 2017). The SWAT-N_2O model provides an opportunity to check if this linearity exists. Our modeling results showed that a linear relationship did exist for first-order to fourth-order streams (Figures 10a and 10d). However, no linear relationship existed between $[N_2O]$ and N_2O emissions on the annual scale, reflecting strong influence of the gas transfer velocity on the N_2O emissions (Figures 10b and 10e). A linear relationship was found between stream nitrate load and N_2O emissions on the annual scale (Figures 10c and 10f), perhaps because stream nitrate load reflects the combined influence of $[NO_3^-]$ and stream discharge, the latter of which strongly affects the gas transfer velocity.

4.5. Uncertainty Analysis

Uncertainties in hydrological modeling stem from model structure, parameters, and observational data for calibration and validation (Fu et al., 2013, 2015), and the present study is no exception. Compared to the direct N_2O emissions from land surface, the understanding about the mechanism of indirect N_2O emissions from streams is still limited, resulting in large uncertainties in the modeling of indirect emissions. For example, the $[N_2O]$ was calculated based only on stream $[NO_3^-]$ in the present study, while $[N_2O]$ may be influenced by many other environmental factors, such as temperature (Hinshaw & Dahlgren, 2013), dissolved oxygen (Rosamond et al., 2011, 2012; Venkiteswaran et al., 2014), streambed morphology (Marzadri et al.,

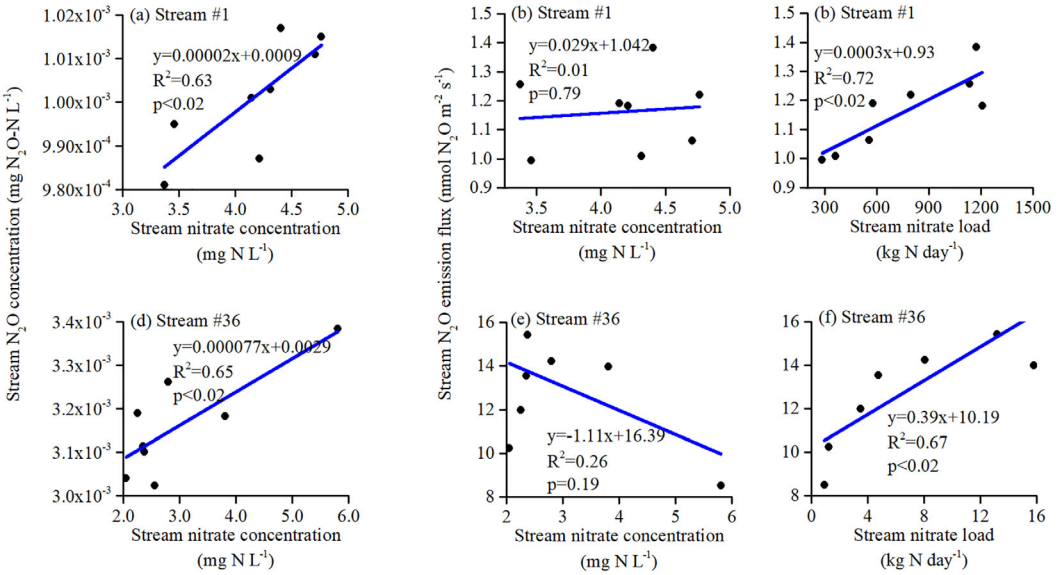

Figure 10. Correlations between modeled mean annual stream nitrate, nitrous oxide concentrations, and indirect N_2O emission fluxes from two streams. Each dot represents an annual mean value from 2007 to 2011 for stream #1 or # 36 (Figure 1e). Streams #1 and # 36 are examples of the fourth-order and first-order streams, respectively.

2014], ratio of ammonium concentration to [NO_3^-] (Marzadri et al., 2011, 2017), and particulate and dissolved organic carbon (Firestone & Davidson, 1989; Harrison & Matson, 2003) in stream water. Although the influences of streambed morphology and stream water temperature on the gas transfer velocity have already been considered, these environmental factors have not been reflected in the present modeling of [N_2O]. Recent studies reported that the hyporheic-benthic zone and the benthic-water column zone are the primary sources of N_2O emissions for the headwater streams and rivers, respectively (Marzadri et al., 2017). It is also possible that the mechanisms affecting [N_2O] and N_2O emissions might be different for different watersheds. The model structure in this study can be improved when more field measurements (e.g., gas transfer velocity, flow velocity, temperature, dissolved oxygen, water turbidity, organic carbon) become available.

Further attention needs to be paid to the simulated small multiyear average [NO_3^-] (e.g., $<$3 mg NO_3-N L^{-1}) for streams with small collecting areas (e.g., $<$10 km^2) (Figure 5). In the current model, the simulated low [NO_3^-] was attributed to high nitrate percolation into groundwater storage, a mechanism that needs verification by field investigation. The simulated stream [NO_3^-] is expected to decrease faster with the increase of stream order if no high nitrate percolation is found.

The second kind of uncertainty was caused by parameter set choice. To illustrate the difference in the simulated results using different parameter sets, two parameter sets (Exp1 and Exp2 in Table 1) were compared in terms of stream [NO_3^-] and N_2O emissions. The modeling statistics such as NSE and R^2 are slightly different, i.e., daily NSE (R^2) for [NO_3^-] is 0.21 (0.36) and 0.32 (0.41) from Exp2 and Exp1, respectively. Although the calibration of Exp1 for first-order stream emissions was based on observation during June, 2013, and the calibration of Exp2 was based on the average emissions during June–August, 2013 and June, 2014, the simulated mean annual emissions from zero and first-order to fourth-order streams are quite close (Exp1: 0.018 nmol m^{-2} s^{-1}; Exp2: 0.020 nmol m^{-2} s^{-1}). Zero-order streams are not continuous in time. In these streams water level, redox conditions, and N_2O production can be highly episodic. Extrapolation of emissions from nonepisodic first and higher-order streams to emissions from zero-order streams may introduce uncertainty to the calculations.

Quality of observation data also introduced uncertainty in this modeling study. Precipitation and flow generation heavily influence the modeled stream [NO_3^-]. The meteorological data used to drive the model were reanalysis data produced by NCEP (section 2.2.1), and the possible inconsistency between the reanalysis precipitation time and amount and the actual values may have contributed to the underestimation of [NO_3^-] in the fall in 2007, 2010, and 2011 in Figure 4. Lack of spatially explicit data on fertilizer application rate, timing, and depth and crop rotation across the model domain also contributed to the uncertainty in the modeled stream [NO_3^-], and the influences of such data shortage on the evaluation of IPCC emission factor for

streams (underestimated by 3.2–5.7 times) need further analysis. We implemented a modeling experiment in which the fertilizer application timing was moved from April 25 to March 15, and found only slight change in the underestimated IPCC emission factor (from 3.15–5.73 to 3.18–5.79). In addition, the calibration for the stream N_2O emissions was based on the area-average data (supporting information Figure S1) that may have slightly different soil properties from those of the study catchment.

5. Summary

In this study, we have extended SWAT for N_2O flux simulations by developing direct and indirect N_2O emission modules and a calibration module, and have implemented the model to a fourth-stream-order catchment and six first-order stream catchments in southeastern Minnesota. The key findings include:

1. The modeled stream N_2O emissions decline exponentially with increasing stream order due to decreases of both the stream nitrate concentration and the gas transfer velocity with increasing stream order.
2. Zero-order streams are predicted to be large N_2O emission hot spots, contributing about 14–27% to the total annual emissions from the Little Cannon River Catchment.
3. Clear spatial patterns are identified for both direct and indirect emissions across the catchment. Important drivers of these patterns are local slope and soil texture.
4. Spatially, negative correlations exist between the direct soil and the indirect stream emissions across the subbasins of the catchment.
5. Our results suggest that the IPCC N_2O emission factor for streams in the Corn Belt should be increased by 3.2–5.7 times.

Overall, the mechanisms controlling N_2O emissions from zero-order and first-order streams are still not completely known. Further, only a limited number of watershed-scale modeling studies have been implemented to study this problem. Additional field studies and better observations are needed to reduce the uncertainties introduced by the model structure, parameter calibration, and lack of observational data. In particular, data on flow velocity, nitrate and N_2O concentrations and gas transfer velocity in stream water, and N_2O fluxes from the hyporheic-benthic zone and at the stream surface are needed to improve the accuracy and reliability of the model.

Acknowledgments
This study was funded by grants supported by the United States Department of Agriculture grant USDA-NIFA 2013–67019-21364 and the Pioneer Hundred Talent Program, Chinese Academy of Sciences (Y7BR021001). This research used resources of the National Energy Research Scientific Computing Center, a DOE Office of Science User Facility supported by the Office of Science of the U.S. Department of Energy under Contract DE-AC02–05CH11231. The Digital Elevation Model (DEM) is obtained from the National Elevation Dataset (https://nationalmap.gov/3DEP/3dep_prodserv.html). The meteorological forcing data are obtained from the National Centers for Environmental Prediction (NCEP) (http://globalweather.tamu.edu/). The streamflow and nitrate concentration data at the outlet of LCRC are obtained from the Minnesota Department of Natural Resources (http://www.dnr.state.mn.us/waters/csg/index.html). The stream N_2O emission data are hosted at http://www.biometeorology.umn.edu/research/data-archives.

References

Alexander, R. B., Smith, R. A., & Schwarz, G. E. (2000). On the delivery of nitrogen to the Gulf of Mexico. *Nature*, *403*, 758–761.

Arnold, J. G., Moriasi, D. N., Gassman, P. W., Abbaspour, K. C., White, M. J., Srinivasan, R., et al. (2012). SWAT: Model use, calibration, and validation. *Transactions of the ASABE*, *55*(4), 1494–1508.

Arnold, J. G., Srinivasan, R., Muttiah, R. S., & Williams, J. R. (1998). Large-area hydrologic modeling and assessment. Part I: Model development. *Journal of the American Water Resources Association*, *34*(1), 73–89.

Baker, J. M., Griffis, T. J., & Ochsner, T. E. (2012). Coupling landscape water storage and supplemental irrigation to increase productivity and improve environmental stewardship in the U.S. Midwest. *Water Resources Research*, *48*, W05301. https://doi.org/10.1029/2011WR011780

Baulch, H. M., Dillon, P. J., Maranger, R., Venkiteswaran, J. J., Wilson, H. F., & Schif, S. L. (2012). Night and day: Short-term variation in nitrogen chemistry and nitrous oxide emissions from streams. *Freshwater Biology*, *57*, 509–525. https://doi.org/10.1111/j.1365-2427.2011.02720.x

Baulch, H. M., Schiff, S. L., Maranger, R., & Dillon, P. J. (2011). Nitrogen enrichment and the emission of nitrous oxide from streams. *Global Biogeochemical Cycles*, *25*, GB4013. https://doi.org/10.1029/2011GB004047

Beaulieu, J. J., Nietch, C. T., & Young, J. L. (2015). Controls on nitrous oxide production and consumption in reservoirs of the Ohio River Basin. *Journal of Geophysical Research: Biogeosciences*, *120*, 1995–2010. https://doi.org/10.1002/2015JG002941

Beaulieu, J. J., Shuster, W. D., & Rebholz, J. A. (2010). Nitrous oxide emissions from a large, impounded river: The Ohio River. *Environmental Science & Technology*, *44*(19), 7527–7533.

Beaulieu, J. J., Tank, J. L., Hamilton, S. K., Wollheim, W. M., Hall, R. O. Jr., Mulholland, P. J., et al. (2011). Nitrous oxide emission from denitrification in stream and river networks. Nitrous oxide emission from denitrification in stream and river networks. *Proceedings of the National Academy of Sciences of the United States of America*, *108*, 214–219.

Bierman, P. M., Rosen, C. J., Venterea, R. T., & Lamb, J. A. (2012). Survey of nitrogen fertilizer use on corn in Minnesota. *Agricultural Systems*, *109*, 43–52.

Billen, G., Thieu, V., Garnier, J., & Silvestre, M. (2009). Modelling the N cascade in regional watersheds: The case study of the Seine, Somme and Scheldt rivers. *Agriculture, Ecosystems & Environment*, *133*, 234–246.

Center for Agricultural and Rural Development (CARD) (2017). *SWAT journal article literature database*. Retrieved from https://www.card.iastate.edu/swat_articles/, accessed on 6 March 2017

Chen, J., Cao, W., Cao, D., Huang, Z., & Liang, Y. (2015). Nitrogen loading and nitrous oxide emissions from a river with multiple hydroelectric reservoirs. *Bulletin of Environmental Contamination and Toxicology*, *94*, 633–639.

Chen, Z., Griffis, T. J., Millet, D. B., Wood, J., Lee, X., Baker, J. M., et al. (2016). Partitioning N_2O emissions within the US Corn Belt using an inverse modeling approach. *Global Biogeochemical Cycles*, *30*, 1192–1205.

Clough, T. J., Bertram, J. E., Sherlock, R. R., Leonard, R. L., & Nowicki, B. L. (2006a). Comparison of measured and EF5-r-derived N_2O fluxes from a spring-fed river. *Global Change Biology*, *12*(2), 352–363. https://doi.org/10.1111/j.1365-2486.2005.01089.x

Clough, T. J., Buckthought, L. E., Casciotti, K. L., Kelliher, F. M., & Jones, P. K. (2006b). Nitrous oxide dynamics in a Braided River System, New Zealand. *Journal of Environmental Quality*, *40*(5), 1532–1541. https://doi.org/10.2134/jeq2010.0527

Clough, T. J., Buckthought, L. E., Kelliher, F. M., & Sherlock, R. R. (2007). Diurnal fluctuations of dissolved nitrous oxide (N_2O) concentrations and estimates of N_2O emissions from a spring-fed river: Implications for IPCC methodology. *Global Change Biology*, *13*(5), 1016–1027. https://doi.org/10.1111/j.1365-2486.2007.01337.x

De Klein, C., Novoa, R. S. A., Ogle, S., Smith, K. A., Rochette, P., & Wirth, T. C. (2006). *N_2O emissions from managed soils, and CO_2 emissions from lime and urea application. IPCC Guidelines for National Greenhouse Gas Inventories*. Prepared by the National Greenhouse Gas Inventories Programme (Vol. 4, pp. 1–54). Hayama, Japan: Institute for Global Environmental Strategies.

del Grosso, S. J., Parton, W. J., Mosier, A. R., Ojima, D. S., Kulmala, A. E., & Phongpan, S. (2000). General model for N_2O and N_2 gas emissions from soils due to dentrification. *Global Biogeochemical Cycles*, *14*(4), 1045–1060. https://doi.org/10.1029/1999GB001225

Denman, K., Brasseur, G., Chidthaisong, A., Ciais, P., Cox, P. M., Dickinson, R. E., et al. (2007). Couplings between changes in the climate system and biogeochemistry. In *Climate change 2007: The physical science basis. Contribution of working group I to the fourth assessment report of the intergovernmental panel on climate change* (pp. 499–587). Cambridge, UK: Cambridge University Press.

Firestone, M. K., & Davidson, E. A. (1989). Microbiological basis of NO and N_2O production and consumption in soil. In M. Andreae & D. Schimel (Eds.), *Exchange of trace gases between terrestrial ecosystems and the atmosphere* (pp. 7–21). New York, NY: John Wiley & Sons.

Fu, C., Chen, J., Jiang, H., & Dong, L. (2013). Threshold behavior in a fissured granitic catchment in southern China. 2: Modeling and uncertainty analysis. *Water Resources Research*, *49*, 2536–2551. https://doi.org/10.1002/wrcr.20193

Fu, C., James, A., & Yao, H. (2014). SWAT-CS: Revision and testing of SWAT for Canadian Shield catchments. *Journal of Hydrology*, *511*, 719–735.

Fu, C., James, A., & Yao, H. (2015). Investigations of uncertainty in SWAT hydrologic simulations: A case study of a Canadian Shield catchment. *Hydrological Processes*, *29*, 4000–4017.

Gaillard, R., Duval, B. D., Osterholz, W. R., & Kucharik, C. J. (2016). Simulated effects of soil texture on nitrous oxide emission factors from corn and soybean agroecosystems in Wisconsin. *Journal of Environmental Quality*, *45*(5), 1540–1548.

Gardner, J. R., Fisher, T. R., Jordan, T. E., & Knee, K. L. (2016). Balancing watershed nitrogen budgets: Accounting for biogenic gases in streams. *Biogeochemistry*, *127*(2–3), 231–253. https://doi.org/10.1007/s10533-015-0177-1

Garnier, J., Billen, G., Vilain, G., Martinez, A., Silvestre, M., Mounier, E., et al. (2009). Nitrous oxide (N_2O) in the seine river and basin: Observations and budgets. *Agriculture, Ecosystems & Environment*, *133*, 223–233.

Griffis, T. J., Chen, Z., Baker, J. M., Wood, J. D., Millet, D. B., Lee, X., et al. (2017). Nitrous oxide emissions are enhanced in a warmer and wetter world. *Proceedings of the National Academy of Sciences of the United States of America*, *114*(45), 12081–12085. https://doi.org/10.1073/pnas.1704552114

Griffis, T. J., Lee, X., Baker, J. M., Russelle, M. P., Zhang, X., Venterea, R., et al. (2013). Reconciling the differences between top-down and bottom-up estimates of nitrous oxide emissions for the U.S. Corn Belt. *Global Biogeochemical Cycles*, *27*, 746–754. https://doi.org/10.1002/gbc.20066

Grossel, A., Nicoullaud, B., Bourennane, H., Lacoste, M., Guimbaud, C., Robert, C., et al. (2016). The effect of tile-drainage on nitrous oxide emissions from soils and drainage streams in a cropped landscape in Central France. *Agriculture, Ecosystems & Environment*, *230*, 251–260.

Gu, J., Nicoullaud, B., Rochette, P., Grossel, A., Henault, C., Cellier, P., et al. (2013). A regional experiment suggest that soil texture is a major control of N_2O emissions from tile drained winter wheat fields during the fertilization period. *Soil Biology and Biochemistry*, *60*, 131–141.

Gupta, H. V., Sorooshian, S., & Yapo, P. O. (1999). Status of automatic calibration for hydrologic models: Comparison with multilevel expert calibration. *Journal of Hydrologic Engineering*, *4*(2), 135–143.

Hall, B. D., Dutton, G. S., & Elkins, J. W. (2007). The NOAA nitrous oxide standard scale for atmospheric observations. *Journal of Geophysical Research*, *112*, D09305. https://doi.org/10.1029/2006JD007954

Hama-Aziz, Z. Q., Hiscock, K. M., & Cooper, R. J. (2017). Indirect nitrous oxide emission factors for agricultural field drains and headwater streams. *Environmental Science & Technology*, *51*, 301–307.

Harrison, J., & Matson, P. (2003). Patterns and controls of nitrous oxide emissions from waters draining a subtropical agricultural valley. *Water Resources Research*, *17*(3), 1080. https://doi.org/10.1029/2002GB001991

Harrison, J., Matson, P., & Fendorf, S. E. (2005). Effects of a diel oxygen cycle on nitrogen transformations and greenhouse gas emissions in a eutrophied subtropical stream. *Aquatic Sciences*, *67*, 308–315.

Hinshaw, S. E., & Dahlgren, R. A. (2013). Dissolved nitrous oxide concentrations and fluxes from the eutrophic San Joaquin River, California. *Environmental Science & Technology*, *47*(3), 1313–1322. https://doi.org/10.1021/es301373h

Hofmann, D. J., Butler, J. H., Dlugokencky, E. J., Elkins, J. W., Masarie, K., Montzka, S. A., et al. (2006). The role of carbon dioxide in climate forcing from 1979–2004: Introduction of the annual greenhouse gas index. *Tellus, Series B*, *58*, 614–619.

Homer, C. G., Dewitz, J. A., Yang, L., Jin, S., Danielson, P., Xian, G., et al. (2015). Completion of the 2011 National Land Cover Database for the conterminous United States-Representing a decade of land cover change information. *Photogrammetric Engineering and Remote Sensing*, *81*(5), 345–354.

Kemanian, A. R., & Stöckle, C. O. (2010). C-Farm: A simple model to estimate the carbon balance of soil profiles. *European Journal of Agronomy*, *32*, 22–29.

Laursen, A. E., & Seitzinger, S. P. (2004). Diurnal patterns of denitrification, oxygen consumption and nitrous oxide production in rivers measured at the whole-reach scale. *Freshwater Biology*, *49*(11), 1448–1458. https://doi.org/10.1111/j.1365-2427.2004.01280.x

Li, C., Aber, J., Stange, F., Butterbach-Bahl, K., & Papen, H. (2000). A process-oriented model of N_2O and NO emissions from forest soils. 1: Model development. *Journal of Geophysical Research*, *105*(D4), 4369–4384.

Marzadri, A., Dee, M. M., Tonina, D., Bellin, A., & Tank, J. L. (2017). Role of surface and subsurface processes in scaling N_2O emissions along riverine networks. *Proceedings of the National Academy of Sciences of the United States of America*, *114*(17), 4330–4335.

Marzadri, A., Tonina, D., & Bellin, A. (2011). A semianalytical three-dimensional process-based model for hyporheic nitrogen dynamics in gravel bed rivers. *Water Resources Research*, *47*, W11518. https://doi.org/10.1029/2011WR010583

Marzadri, A., Tonina, D., Bellin, A., & Tank, J. L. (2014). A hydrologic model demonstrates nitrous oxide emissions depend on streambed morphology. *Geophysical Research Letters*, *41*, 5484–5491. https://doi.org/10.1002/2014GL060732

McElroy, A. D., Chiu, S. Y., Nebgen, J. W., Aleti, A., & Bennett, F. W. (1976). *Loading functions for assessment of water pollution from nonpoint sources* (EPA document EPA 600/2–76-151). Athens, GA: USEPA.

McMahon, P. B., & Dennehy, K. F. (1999). N_2O emission from a nitrogen-enriched river. *Environmental Science & Technology*, *33*(303), 21–25.

Memorandum of Minnesota Pollution Control Agency (2014). *Little Cannon River watershed SWAT modeling*. Memorandum prepared by LimnoTech for the Minnesota Pollution Control Agency. June 20, 2014.
Memorandum of Minnesota Pollution Control Agency (2015). *Cannon River watershed HSPF model development project—Phase II*. Memorandum prepared by LimnoTech for the Minnesota Pollution Control Agency. November 18, 2015.
Miller, S. M., Kort, E. A., Hirsch, A. I., Dlugokencky, E. J., Andrews, A. E., Xu, X., et al. (2012). Regional sources of nitrous oxide over the United States: Seasonal variation and spatial distribution. *Journal of Geophysical Research*, *117*, D06310. https://doi.org/10.1029/2011JD016951
Moriasi, D. N., Arnold, J. G., Van Liew, M. W., Bingner, R. L., Harmel, R. D., & Veith, T. L. (2007). Model evaluation guidelines for systematic quantification of accuracy in watershed simulations. *Transactions of the ASABE*, *50*(3), 885–900.
Mulla, D. J., Birr, A. S., Kitchen, N., & David, M. (2005, 26–28 September). Evaluating the effectiveness of agricultural management practices at reducing nutrient losses to surface waters. In *Proceedings of the Gulf Hypoxia and local water quality concerns workshop*, Ames, Iowa (pp. 171–193).
Nash, J. E., & Sutcliffe, J. V. (1970). River flow forecasting through conceptual models, Part I: A discussion of principles. *Journal of Hydrology*, *10*, 282–290.
National Resource Conservation Service (NRCS) (2006). *Land resource regions and major land resource areas of the United States, the Caribbean, and the Pacific Basin* (Vol. 296, 682 p.). Washington, DC: United States Department of Agriculture Handbook. United States Department of Agriculture.
National Resource Inventory (1992). *Subsurface drains on agricultural land in the conterminous United States* (National Resource Inventory Conservation Practice 606). Reston, VA: U.S. Geological Survey.
Neitsch, S. L., Arnold, J. G., Kiniry, J. R., & Williams, J. R. (2005). *Soil and water assessment tool theoretical documentation version 2005*. Texas: Temple. Retrieved from https://swat.tamu.edu/media/1292/SWAT2005theory.pdf
Neitsch, S. L., Arnold, J. G., Kiniry, J. R., & Williams, J. R. (2011). *Soil and water assessment tool theoretical documentation version 2009* (Technical Report No. 406). College Station, Texas: Texas Water Resources Institute. Retrieved from http://hdl.handle.net/1969.1/128050
Neitsch, S. L., Arnold, J. G., Kiniry, J. R., Williams, J. R., & King, K. W. (2002). *Soil and Water Assessment Tool theoretical documentation version 2000*. (TWRI Report TR-191). College Station, Texas: Texas Water Resources Institute.
Nevison, C. (2000). Review of the IPCC methodology for estimating nitrous oxide emissions associated with agricultural leaching and runoff. *Chemosphere: Global Change Science*, *2*(3–4), 493–500.
Oleson, K., Lawrence, D. M., Bonan, G. B., Drewniak, B., Huang, M., Koven, C. D., et al. (2013). *Technical description of version 4.5 of the Community Land Model (CLM)* (NCAR Tech. Note NCAR/TN-503+STR, 420 p.). Boulder, CO: National Center for Atmospheric Research.
Parajuli, P. B., Nelson, N. O., Frees, L. D., & Mankin, K. R. (2009). Comparison of AnnAGNPS and SWAT model simulation results in USDA-CEAP agricultural watersheds in south-central Kansas. *Hydrological Processes*, *23*, 748–763.
Parton, W. J., Ojima, D. S., Cole, C. V., & Schimel, D. S. (1994). *A general model for soil organic matter dynamics: Sensitivity to litter chemistry, texture and management. Quantitative modeling of soil forming processes* (Spec. Publ. 39, pp. 147–67). Madison, WI: Soil Science Society of America.
Prather, M. J., Holmes, C. D., & Hsu, J. (2012). Reactive greenhouse gas scenarios: Systematic exploration of uncertainties and the role of atmospheric chemistry. *Geophysical Research Letters*, *39*, L09803. https://doi.org/10.1029/2012GL051440
Prather, M. J., Hsu, J., DeLuca, N. M., Jackman, C. H., Oman, L. D., Douglass, A. R., et al. (2015). Measuring and modeling the lifetime of nitrous oxide including its variability. *Journal of Geophysical Research: Atmospheres*, *120*, 5693–5705.
Quick, A. M., Reeder, W. J., Farrell, T. B., Tonina, D., Feris, K. P., & Benner, S. G. (2016). Controls on nitrous oxide emissions from the hyporheic zones of streams. *Environmental Science & Technology*, *50*(21), 11491–11500.
Ravishankara, A. R., Daniel, J. S., & Portmann, R. W. (2009). Nitrous oxide: The dominant ozone-depleting substance emitted in the 21st century. *Science*, *326*, 123–125.
Raymond, P. A., Zappa, C. J., Butman, D., Bott, T. L., Potter, J., Mulholland, P., et al. (2012). Scaling the gas transfer velocity and hydraulic geometry in streams and small rivers. *Limnology and Oceanography Methods*, *2*, 41–53. https://doi.org/10.1215/21573689-1597669
Reay, D. S. Davidson, E. A., Smith, K. A., Smith, P., Melillo, J. M., Dentener, F., et al. (2012). Global agriculture and nitrous oxide emissions. *Nature Climate Change*, *2*, 410–416.
Reay, D. S., Smith, K. A., & Edwards, A. C. (2003). Nitrous oxide emission from agricultural drainage waters. *Global Change Biology*, *9*(2), 195–203.
Rosamond, M. S., Thuss, S. J., & Schiff, S. L. (2012). Dependence of riverine nitrous oxide emissions on dissolved oxygen levels. *Nature Geoscience*, *5*, 715–718.
Rosamond, M. S., Thuss, S. J., Schiff, S. L., & Elgood, R. J. (2011). Coupled cycles of dissolved oxygen and nitrous oxide in rivers along a trophic gradient in southern Ontario, Canada. *Journal of Environmental Quality*, *40*(1), 256–270.
Saikawa, E., Prinn, R. G., Dlugokencky, E., Ishijima, K., Dutton, G. S., Hall, B. D., et al. (2014). Global and regional emissions estimates for N_2O. *Atmospheric Chemistry and Physics*, *14*, 4617–4641.
Sander, R. (1999). *Compilation of Henry's Law constants for inorganic and organic species of potential importance in environmental chemistry, version 3*, 8 April 1999. Mainz, Germany: Max-Planck Institute of Chemistry, Air Chemistry Department. Retrieved from http:\\www.mpch-mainz.mpg.de\~sander\res\henry.html
Skiba, U., & Ball, B. (2002). The effect of soil texture and soil drainage on emissions of nitric oxide and nitrous oxide. *Soil Use and Management*, *18*, 56–60.
Snider, D. M., Venkiteswaran, J. J., Schiff, S. L., & Spoelstra, J. (2015). From the ground up: Global nitrous oxide sources are constrained by stable isotope values. *PLoS ONE*, *10*(3), e0118954. https://doi.org/10.1371/journal.pone.0118954
Soued, C., del Giorgio, P. A., & Maranger, R. (2016). Nitrous oxide sinks and emissions in boreal aquatic networks in Québec. *Nature Geoscience*, *9*, 116–120. https://doi.org/10.1038/ngeo2611
Thieu, V., Billen, G., & Garnier, J. (2009). Nutrient transfer in three contrasting N-W European watersheds: The Seine, Somme and Scheldt rivers. A comparative application of the Seneque/Riverstrahler model. *Water Research*, *43*, 1740–1754.
Turner, P. A., Griffis, T. J., Baker, J. M., Lee, X., Crawford, J. T., Loken, L. C., et al. (2016). Regional-scale controls on dissolved nitrous oxide in the Upper Mississippi River. *Geophysical Research Letters*, *43*, 4400–4407. https://doi.org/10.1002/2016GL068710
Turner, P. T., Griffis, T. J., Lee, X., Baker, J. M., Venterea, R. T., & Wood, J. D. (2015). Indirect nitrous oxide emissions from streams within the US Corn Belt scale with stream order. *Proceedings of the National Academy of Sciences of the United States of America*, *112*(32), 9839–9843.
US Department of Agriculture-Natural Resource Conservation Service (USDA-NRCS) (1992). *State Soil Geographic Database (STATSGO) Data Users' Guide* (Publ. 1492). Washington, DC: U.S. Government Printing Office.

USDA Soil Conservation Service (1972). *National engineering handbook section 4 Hydrology* (Chapters 4 − 10). Washington DC: USDA Soil Conservation Service.

Venkiteswaran, J. J., Rosamond, M. S., & Schiff, S. L. (2014). Nonlinear response of riverine N_2O fluxes to oxygen and temperature. *Environmental Science & Technology*, *48*(2), 1566–1573. https://doi.org/10.1021/es500069j

Wellen, C., Kamran-Disfani, A., & Arhonditsis, G. B. (2015). Evaluation of the current state of distributed watershed nutrient water quality modeling. *Environmental Science & Technology*, *49*, 3278–3290.

Yan, W., Yang, L., Wang, F., Wang, J., & Ma, P. (2012). Riverine N_2O concentrations, exports to estuary and emissions to atmosphere from the Changjiang River in response to increasing nitrogen loads. *Global Biogeochemical Cycles*, *26*, GB4006. https://doi.org/10.1029/2010GB003984

Zhang, X., Izaurralde, R. C., Arnold, J. G., Williams, J. R., & Srinivasan, R. (2013). Modifying the Soil and Water Assessment Tool to simulate cropland carbon flux: Model development and initial evaluation. *Science of the Total Environment*, *463–464*, 810–822.

Zhang, X., Srinivasan, R., & Van Liew, M. (2008). Multi-site calibration of the SWAT model for hydrologic modeling. *Transactions of the ASABE*, *51*(6), 2039–2049.